https://ntrs.nasa.gov/search.jsp?R=19930082159 2018-02-13T18:16:46+00:00Z

1192

NATIONAL ADVISORY COMMITTEE FOR AERONAUTICS

TECHNICAL NOTE

No. 1192

CHARTS SHOWING RELATIONS AMONG PRIMARY AERODYNAMIC VARIABLES FOR HELICOPTER-PERFORMANCE ESTIMATION

By Herbert W. Talkin

Langley Memorial Aeronautical Laboratory
Langley Field, Va.

FAIRCHILD AIRCRAFT PROPERTY
ENGINEERING DEPARTMENT

PROPERTY FAIRCHILD
ENGINEERING LIBRARY

CASE FILE
COPY

Washington
February 1947

NATIONAL ADVISORY COMMITTEE FOR AERONAUTICS

TECHNICAL NOTE No. 1192

CHARTS SHOWING RELATIONS AMONG PRIMARY AERODYNAMIC VARIABLES FOR HELICOPTER-PERFORMANCE ESTIMATION

By Herbert W. Talkin

SUMMARY

In order to facilitate solutions of the general problem of helicopter selection, the aerodynamic performance of rotors is presented in the form of charts showing relations between primary design and performance variables. By the use of conventional helicopter theory, certain variables are plotted and other variables are considered fixed. Charts constructed in such a manner show typical results, trends, and limits of helicopter performance. Performance conditions considered include hovering, horizontal flight, climb, and ceiling. Special problems discussed include vertical climb and the use of rotor-speed-reduction gears for hovering.

INTRODUCTION

The general problem of helicopter design may be conveniently broken down into that of obtaining suitable compromises among the requirements imposed by considerations of structures, vibration, and aerodynamics. The object of the present paper is to provide assistance for obtaining solutions for the part of the design problem relating to aerodynamics. These solutions are presented in the form of graphical charts showing the trends and differences in performance with changes in values of the aerodynamic design variables.

The charts herein are synthesized from the elementary charts of reference 1 by the choice of typical values for certain design variables and by plotting the relations among the remaining variables. The quantity held fixed for most of the plots is an

average lift-drag ratio for the rotor-blade sections. Charts are plotted for each performance characteristic on coordinates of the primary parameters power loading and disk loading. Correlation between the performance indicated by the charts and the performance that may be realized in practice is chiefly dependent on a knowledge of the profile-drag coefficient of the blade under flight conditions. The determination of this coefficient is not a part of the present paper, which is restricted to showing the relations among the other aerodynamic variables and the variation of these relations with rotor-blade-element lift coefficient and rotor-blade-element profile-drag coefficient.

The accuracy and applicability of results obtained from the charts are subject to the following conditions and limitations:

(1) The charts are constructed from theoretically derived relationships. Although adequate experimental data are unavailable for detailed checking, no definite discrepancies have been observed in existing data such as reference 2. The theory is considered fully satisfactory for the study of trends and of differences in performance with change in design. The scope of the present paper does not include all the aerodynamic information needed for actually selecting optimum aerodynamic designs because the rotor-blade average effective profile-drag coefficient δ is held constant. Thus for cases in which the value of δ would vary with a design variable, this variation is not shown.

(2) The power used in the power-loading parameter is that delivered to the lifting rotor. Transmission losses, engine cooling power, tail rotor power, or other auxiliary power requirements are not included. In the helicopter of reference 2, for example, these auxiliary losses aggregate some 15 percent.

(3) The charts apply directly to helicopters with a single lifting rotor comprised of three blades. When counter-rotating rotors are used, part of the rotational energy may be considered removed from the slipstream. The rotational energy in the wake of a single rotor, as well as the induced-flow effect of the blade tip, may be estimated from reference 1; each is generally less than 1 percent of the rotor power. With multiple noncoaxial rotors, the helicopter performance may be approximated by calculating each rotor independently with its proportionate part of the gross weight and the fuselage drag. This approximation would neglect the induced interference between rotors, which depends on the geometrical arrangement.

(4) Certain factors tend to reduce the performance of helicopters. Among these are blade deformation under load, rotor

coning, and hub interference. With careful design, these factors can be made small or constant and need not therefore influence the study of performance trends with design changes.

Derviations of the charts are explained in the appendix.

SYMBOLS

A rotor-disk area, square feet

b number of blades in rotor disk

c blade chord, feet

C_{D_f} fuselage drag coefficient along flight path, exclusive of rotor blades, based on rotor-disk area A $\left(C_{D_f} = \frac{f}{A}\right)$

c_{d_o} rotor-blade-element profile-drag coefficient

c_l rotor-blade-element lift coefficient

C_T thrust coefficient $\left(\frac{T}{\rho A(\Omega R)^2}\right)$

F power-loading parameter for any flight path $\left(\frac{P}{W}\sqrt{\frac{A}{W}\frac{\rho}{\rho_0}}\right)$

F_b increase in F due to finite-blade number

F_{rot} increase in F due to slipstream rotation

f fuselage equivalent flat-plate area based on unit drag

L/D lift-drag ratio

P rotor power, horsepower

R rotor-disk radius, feet

r radius to a point on rotor blade, feet

T rotor thrust, assumed equal to W, pounds

v induced axial velocity in rotor disk, feet per second

V velocity of helicopter along its flight path, feet per second unless otherwise indicated

V_c rate of climb in forward flight, feet per second unless otherwise indicated

W gross weight of helicopter minus fuselage lift, pounds

W/A disk loading

W/P power loading

x radius ratio $\left(\frac{r}{R}\right)$

Y helicopter velocity parameter $\left(V\sqrt{\frac{A}{W}\frac{\rho}{\rho_0}}\right)$

Y_c helicopter rate-of-forward-climb parameter $\left(V_c\sqrt{\frac{A}{W}\frac{\rho}{\rho_0}}\right)$

Y_{best} value of Y_h for minimum F_h

Y_t rotor tip-speed parameter $\left(\Omega R\sqrt{\frac{A}{W}\frac{\rho}{\rho_0}}\right)$ or $\left(\frac{1}{\sqrt{\rho_0 C_T}}\right)$

δ rotor-blade average effective profile-drag coefficient

$\lambda = \frac{v}{\Omega R}$

μ tip-speed ratio; that is, ratio of horizontal velocity of helicopter to rotational tip speed of rotor $\left(\mu = \frac{Y_h}{Y_t} = \frac{V_h}{\Omega R}\right)$

ρ mass density of air at altitude, slug per cubic foot

ρ_0 mass density of air at sea level, 0.002378 slug per cubic foot

σ equivalent rotor solidity $\left(\sigma = \dfrac{\int_0^1 \sigma_x x^3\,dx}{\int_0^1 x^3\,dx} = 4\int_0^1 \sigma_x\, x^3\,dx\right.$

where $\left.\sigma_x = \dfrac{bc_x}{\pi R}\right)$

Ω rotor angular velocity, radians per second

ΩR rotational tip speed, feet per second

Subscripts:

a at altitude

f due to fuselage drag

h for horizontal flight

i induced

0 at sea level

v for vertical flight

x for the radius ratio $\left(\dfrac{r}{R} = x\right)$

δ due to blade profile drag

max maximum

min minimum

PROBLEM OF HELICOPTER SELECTION

Helicopter selection will be considered to mean the selection of values for the aerodynamic design variables that would most nearly obtain a desired performance. Practical considerations require a knowledge of the useful load associated with a given performance, and the useful load is in turn influenced by such

variables as structural efficiency and engine economy. Data for the evaluation of these variables are not available at the present time because the values of the variables are determined primarily by considerations of vibration, safety, control, and comfort, rather than efficiency considerations.

In view of such considerations the problem of helicopter selection for maximum useful load is not considered at the present time to be reducible to the form of useful performance selection charts. Aerodynamic performance charts, however, to show trends with variations in the primary design variables are presented; the importance of blade and fuselage drag is also demonstrated. A basis for an intelligent approach to the selection of balanced designs is thus provided in accordance with the best available engineering data. The problems of range and endurance are associated with the engine-fuel economy and are not directly considered herein.

SPECIALIZED SELECTION CHARTS

Helicopter performance is first illustrated for a conventional design. Figure 1 shows curves for constant values of horizontal velocity V_h plotted on coordinates of power loading W/P against disk loading W/A for helicopters with the following design specifications:

Rotor-disk radius, R, feet	19.0
Equivalent rotor solidity, σ	0.056
Tip-speed parameter $\left(Y_t = \Omega R\sqrt{\frac{A}{W}\frac{\rho}{\rho_0}}\right)$	320
Rotor-blade average effective profile-drag coefficient, δ	0.012
Fuselage equivalent flat-plate area, f, square feet	10.0
Altitude	Sea level
Air density, ρ_0, slug per cubic foot	0.002378

There remain as design variables for this case, therefore, W, P, and V_h, any two of which determine the third and thus define a particular helicopter.

An envelope of the constant velocity curves (fig. 1) represents the maximum power loading that can be sustained in flight at optimum speed. This envelope is labeled $(W/P)_{max}$ in the figures.

The maximum power loading that can be sustained at zero velocity is shown by the short dashed line and is labeled hovering.

If the attainment of maximum power loading were the only object of the design of helicopters with the constants of figure 1, the figure would suggest the use of as low a disk loading as possible. Figure 1 shows that the power loading can be increased as the disk loading is decreased. For a given helicopter power, the rotor size increases with decreased disk loading and, therefore, the rotor weight increases. A compromise between rotor weight and increased power loading would give an optimum disk loading. Since information on the variation of rotor weight with size and solidity is unavailable, this optimum is not shown.

The curves of constant velocity give an optimum disk loading to obtain maximum power loading. This optimum is obtained when the induced drag balances the profile drag. At lower disk loading the profile drag is too high, whereas at higher disk loading the induced drag is the determining factor. The value of this optimum is greatly dependent upon the profile drag attainable in flight. Decreasing the profile drag decreases the optimum disk loading. For low forward speeds the induced drag is so important that the optimum occurs below a disk loading of 1/2 pound per square foot. Since the disk area would be extremely large in this range of disk loading, these optimums are not shown.

Curves of maximum rate of climb are shown in figure 2 and, for comparison, the hovering and the maximum power-loading curves from figure 1. Curves of constant service ceiling (rate of climb, 100 ft/min) are shown in figure 3; also shown are the hovering and the maximum power-loading curves from figure 1. The curves of service ceiling are based on constant rotor revolutions per minute with rotor power proportional to the density. The power-loading scale is for the sea-level condition.

Conclusions drawn from figures 1 to 3 are subject to the constant values arbitrarily assigned to σ, δ, Y_t, R, or f. Attention is called to the fact that the Mach number at the tip of the advancing blade will affect the value of δ; also, the higher values of the tip-speed ratio μ encountered at the higher forward speeds may be impractical from considerations of stability and control. For these and other reasons it is necessary to consider changes that may occur as the fixed quantities are varied. For this purpose, other types of charts are introduced.

PERFORMANCE STUDY CHARTS

The types of charts presented are summarized in table I. The generalized charts are the most compact but in some respects the least convenient to use because they show relations among complex parameters. The power-loading disk-loading charts are more direct reading. In order to facilitate discussion of the parameters used, the elementary design variables to be selected are listed in table II. Specification of the elementary design variables essentially determines the helicopter aerodynamic performance, which may be expressed in terms of the elementary performance variables listed in table III. The large number of the design variables affecting helicopter performance complicates the direct graphical presentation of the effects.

The problem can be simplified by the use of fundamental parameters each representing a significant group of variables. From the analysis of reference 1 the fundamental design parameters of table IV are obtained. The corresponding performance parameters are given in table V.

A comparison of tables II and IV shows that use of the fundamental design parameters reduces the number of variables from seven to four, but although this reduction greatly simplifies graphical presentation it correspondingly complicates the interpretation of the graph. A compromise between the extremes of the elementary and the fundamental design variables may be based on use of the familiar parameters power loading and disk loading. This compromise, however, reduces the number of variables by only one.

Generalized Selection Charts

A generalized selection chart is shown in figure 4. The significance of the chart is best explained by a brief description of its derivation. A fuller derivation for all figures is given in the appendix.

On a simple graph only three variables can be shown. The four fundamental design parameters (table IV) plus δ and a performance parameter make a total of six; consequently, three variables must be fixed. As explained in the "Introduction," constant values have been assigned to δ. The value of δ for a given blade is determined by the average effective rotor-blade-element lift coefficient, which is in turn dependent on the

tip-speed ratio $\mu = \frac{Y_h}{Y_t}$ and the quantity $\sigma Y_t^2 = \frac{\sigma}{\rho_0 C_T}$. Thus, two of these three quantities determine the third and, in general, an optimum combination will exist for each performance requirement. The investigation of this optimum is not however part of the present paper. For the present purpose the value of μ is fixed at 0.3 and the value of σY_t^2, at 5740. As computed from section 8a of reference 1 this value of σY_t^2 corresponds to an average effective rotor-blade-element lift coefficient of approximately 0.44 in hovering.

In figure 4 curves of constant $C_{D_{f_h}}$ are plotted on a logarithmic scale of the reciprocal of the power-loading parameter $\frac{1}{F_h} = \frac{W}{P}\sqrt{\frac{W}{A}\frac{\rho_0}{\rho}}$ against the horizontal-velocity parameter $Y_h = V_h\sqrt{\frac{A}{W}\frac{\rho}{\rho_0}}$ for $\delta = 0.012$. The condition $\sigma Y_t^2 = \frac{\sigma}{\rho_0 C_T} = 5740$ relates the solidity σ to Y_t and therefore to Y_h by the curve of σ against $Y_t = \Omega R\sqrt{\frac{A}{W}\frac{\rho}{\rho_0}}$ shown in the lower part of the figure.

Curves of $\frac{1}{F_h} = \frac{W}{P}\sqrt{\frac{W}{A}\frac{\rho_0}{\rho}}$ against $Y_t = \Omega R\sqrt{\frac{A}{W}\frac{\rho}{\rho_0}}$ for hovering are also shown in figure 4 and cover three conditions, namely, untwisted rectangular blades with $\delta = 0.012$ and uniform disk loading with $\delta = 0.012$ and $\delta = 0.006$. The power required for untwisted blades is only about 4 percent higher than the optimum that is obtained with uniform disk loading. Unless otherwise stated, uniform disk loading is used throughout the present paper. The effect of δ on the power required for hovering is large; however, the effect of δ is about 41 percent greater for $\mu = 0.3$ than for hovering, in accordance with equation 23 of reference 1. This effect is shown by figure 5, which is similar to figure 4 but with $\delta = 0.006$ instead of $\delta = 0.012$.

The restriction of figure 4 to the condition $\mu = 0.3$ fixes the relation between Y_t and Y_h in that $\mu = \frac{Y_h}{Y_t}$, but increasing μ

has comparatively little effect on the curves of $\frac{1}{F_h} = \frac{W}{P}\sqrt{\frac{W}{A}\frac{\rho_0}{\rho}}$ against $Y_h = V_h\sqrt{\frac{A}{W}\frac{\rho}{\rho_0}}$ for constant $C_{D_{f_h}}$ in the neighborhood of $\mu = 0.3$ This fact is illustrated by figure 6 in which $\frac{1}{F_h} = \frac{W}{P}\sqrt{\frac{W}{A}\frac{\rho_0}{\rho}}$ is plotted against μ for $C_{D_{f_h}} = 0.01$ for two values of δ with $Y_h = 75$.

Figures 7 and 8 show curves of constant values of the maximum rate-of-forward-climb parameter Y_c for helicopters of figures 4 and 5, that is, for $\delta = 0.012$ and $\delta = 0.006$, respectively. Besides yielding the maximum rate of climb in forward flight V_c, feet per second, these curves permit calculations of the service ceiling. For example, if the service ceiling is defined as corresponding to the value of ρ/ρ_0 for which the rate of climb is 100 feet per minute, then $V_c = \frac{100}{60} = \frac{5}{3}$. From the value of Y_c corresponding to any point on the figure, the value of ρ/ρ_0 may then be calculated for a given value of the disk loading W/A.

Figure 9 shows curves of $\frac{1}{F_h} = \frac{W}{P}\sqrt{\frac{W}{A}\frac{\rho_0}{\rho}}$ against $Y_t = \Omega R\sqrt{\frac{A}{W}\frac{\rho}{\rho_0}}$ for representative values of Y_v, for two values of the fuselage vertical drag coefficient $\left(C_{D_{f_v}} = 0 \text{ and } 0.1\right)$, and for $\delta = 0.012$. The solidity corresponds to $\sigma Y_t{}^2 = \frac{\sigma}{\rho_0 C_T} = 5740$. The figure shows the small effect of fuselage vertical drag coefficient on the power required for vertical climb. Thus for $C_{D_{f_v}} = 0.1$ the fuselage equivalent flat-plate area in vertical climb is 10 percent of the rotor-disk area, and at $Y_v = 30$ this large fuselage drag increases by only 8 percent the power required. The value $Y_v = 30$ corresponds to a rate of vertical climb of 2700 feet per minute at sea level for $\frac{W}{A} = 2.25$. $\left(Y_v = V_v\sqrt{\frac{A}{W}\frac{\rho}{\rho_0}}\right)$

The effect of δ in vertical climb is similar to its effect in hovering, which is illustrated in figure 4.

The last of the generalized charts is for the rate-of-forward-climb parameter Y_c shown plotted in figure 10 against the difference $F - F_h$ between the power-loading parameter available and that required for horizontal flight at climbing speed. Curves for several values of the velocity parameter in climb Y are shown. This figure is the same as figure 6 of reference 1.

Figures 4 to 10 contain all the essential aerodynamic information within the scope of the present paper. When the disk loading has been selected, these figures show directly the relations among power loading W/P, rotational tip speed ΩR, and horizontal velocity V_h.

Power-Loading Disk-Loading Charts

The effect of the disk loading is best shown by charts in which W/A is one of the coordinates. The disk loading may be varied by independent changes in either the rotor-blade-element lift coefficient, the solidity, or the tip speed. The disk loading was varied by changing the tip speed in figures 1 to 3. Among the remaining variables in these figures the fuselage equivalent flat-plate area f was held constant and the tip-speed ratio μ was allowed to vary. In the charts beginning with figure 11 the disk loading is again varied by changing the tip speed but the value of μ is held constant while the fuselage equivalent flat-plate area is varied. It is to be expected that considerations of minimum profile-drag loss and considerations of stability and control at maximum speed will tend to determine an optimum value of μ.

As has been pointed out, the use of elementary variables in charts increases the number of variables and therefore the number of charts as compared with charts based on fundamental parameters. In the generalized charts, figures 4 to 10, adequate simplification was achieved by fixing the values of μ, δ, $C_{D_{f_h}}$, $C_{D_{f_v}}$, and σY_t^2. In the charts presented as figures 11 to 16, the value of σ also is fixed at 0.056 and the altitude is restricted to sea level. In addition, the fuselage drag is expressed in terms of the ratio f/P.

Figure 11 shows curves for constant values of f/P at sea level on the coordinates of W/P against W/A for $\mu = 0.3$ and $\delta = 0.012$. Also shown are the hovering curve, curves of maximum rate of climb in forward flight, and the region in which the blade tip stalls in high speed. Tip stall was not found to occur for the maximum rates of climb shown in the figures and was determined by stall at maximum horizontal velocity, as explained

in the appendix. The stalls shown should be regarded as a reference condition only, inasmuch as the actual stall depends upon the particular airfoil sections used. The maximum velocity varies with W/A and is shown by the horizontal scale at the top of the graph. The relation between the maximum velocity and the disk loading is fixed by, among other things, the choice of solidity because the values of σY_t^2 and Y_h/Y_t have also been fixed. For higher speeds with a given disk loading, it would therefore be necessary to employ a higher value of Y_t.

The most direct application of figure 11 is as follows: Let it be desired to find how gross weight varies with disk loading for a given engine with rotor power P. The curves of constant f/P in the figure are then equivalent to curves of constant f and the scale of W/P is proportional to the gross weight W. The figure then shows how for a given f the gross weight decreases with increasing disk loading while the maximum speed increases. Inasmuch as these relationships are dependent on the values selected for the fixed quantities, the fixed quantities are changed on subsequent figures (figs. 12 to 16) so that the influence of all the significant design variables may be studied. The selection of the values to be used for the fixed quantities is dependent on data outside the scope of the present paper.

In order to compare the charts for different values of δ, figure 12 is made similar to figure 11 but with half the blade profile-drag coefficient, that is, $\delta = 0.006$. Figures 13 and 14 apply to $\delta = 0.012$ and $\delta = 0.006$, respectively, for $\mu = 0.2$; and figures 15 and 16, to $\delta = 0.012$ and $\delta = 0.006$, respectively, for $\mu = 0.4$. In figures 13 and 14, the region of stall lies below a power loading of 5 and is not shown.

In figures 11 to 16 those helicopters represented by curves above the hovering curve have insufficient power to hover free of the ground effect while those represented by curves below the hovering curve require more power for high-speed flight than for hovering. The first group of helicopters loses the chief advantage of a helicopter, that is, the ability to hover; whereas the second group possesses more power than required for hovering.

Figure 17 shows the power-loading disk-loading characteristics of helicopters possessing power just sufficient to hover for conditions of $\delta = 0.012$ and approximately constant c_l, that is, $\sigma Y_t^2 = 5740$. In order to avoid the confusion of numerous curves, only limiting curves are shown in the figure; that is, the

two solid-line curves define the extremes of fuselage drag coefficient expressed in terms of $\frac{f_h}{P} = 0.01$ and $\frac{f_h}{P} = 0.25$ and the dashed curves are for limiting values of σ of 0.02 and 0.18, respectively. The constant solidity curves are also curves of approximately constant service ceiling, varying from 10,000 to 23,000 feet. Similarly, the curves of constant f/P are also curves of constant rotational tip speed ΩR varying from 325 to 850 feet per second; inasmuch as the value of μ has been fixed at 0.3, these curves are also curves of constant horizontal velocity V_h varying from 66 to 175 miles per hour. Particularly notable in this graph is the small variation in power loading resulting from variations in σ or f/P.

For greater detail, the part of figure 17 bounded by the rectangle is expanded in figure 18 and curves for intermediate values are included also. In addition, curves of maximum rate of climb in forward flight V_c are shown. Data are for sea level in figures 17 and 18; also the value of μ is 0.3 only in high speed since in climb and at service ceiling the speed of the helicopter is that corresponding to the maximum rate of climb.

In general, various requirements will make undesirable the selection of helicopters to fulfill the requirements of figures 17 and 18. The figures are of interest chiefly for showing the relations among the design and performance variables of a class of helicopters that may be regarded as a standard for comparison with special designs.

The foregoing statements, as well as those in connection with most of the other figures, apply to the same condition for δ in hovering as in high speed. Since δ is the rotor-blade average effective profile-drag coefficient, the value of δ will in general change with Mach number and with the tip-speed ratio μ. In order to illustrate the change with μ, the values of δ in hovering and high speed were calculated for σY_t^2, corresponding to a lift-drag ratio L/D for $\mu = 0.3$, and for the three airfoil sections of reference 3. The curves of the airfoil section profile-drag characteristics are plotted in figure 19, and the method used for calculation is explained in the appendix in the discussion of figure 22. The values obtained for δ at $\mu = 0$ and at $\mu = 0.3$ are listed in the following table:

Airfoil / Flight condition	Rough conventional	Smooth NACA 3-H-13.5	Smooth NACA 23015
Hovering ($\mu = 0$)	0.0126	0.0045	0.0087
High speed ($\mu = 0.3$)	.0140	.0063	.0085

The drag coefficient in the hovering condition is constant throughout the entire rotor cycle; whereas in the high-speed condition, the drag coefficient varies with the position of the blade during the cycle since the relative velocity of the airfoil section and the air is constantly changing. The average effective profile-drag coefficient for the entire cycle, therefore, is determined by an integrated average of the drag coefficient throughout the cycle. For this reason the shapes of the lift and profile-drag curves affect the average value for the high-speed condition. The foregoing table demonstrates that the average effective profile-drag coefficient for the entire cycle may be either higher or lower in the high-speed condition than in the hovering condition, depending on the airfoil section characteristics. The effects of varying δ may be estimated by comparing figures 4 and 7 for $\delta = 0.012$ with figures 5 and 8 for $\delta = 0.006$.

Special Purpose Charts

Vertical climb.- A few special problems are of interest. It is often necessary to have available a definite rate of vertical climb. Vertical climb may be obtained either by reducing the gross weight of an existing helicopter or by designing for vertical climb. Figure 20 shows the rate of vertical climb that may be obtained by decreasing the gross weight of a helicopter possessing power just sufficient to hover. Consider a helicopter that has zero rate of climb for a disk loading of 2.5. If the gross weight is reduced 20 percent, the disk loading would be 2 pounds per square foot of disk area and the resulting rate of climb may be read from figure 20 as 850 feet per minute. (Read the figure at 20 percent reduction of gross weight on the curve of $\frac{W}{A} = 2$.) The figure includes several curves for $C_{D_{f_v}} = 0.1$ to show the small

effect on the vertical rate of climb of such a large value for the vertical drag coefficient.

When vertical climb is an essential characteristic of performance, designing for vertical climb may be desirable, which can be done by designing for hovering at some greater gross weight than will be used and reducing the gross weight to obtain the required vertical climb, as given by figure 20. If the helicopter is to be operated always at the reduced gross weight, the solidity should be decreased in the same proportion as the gross weight to obtain the originally chosen value of σY_t^2.

Hovering.- Figure 21 shows curves of constant tip speed for hovering on the power-loading disk-loading coordinates crossed by curves of constant solidity. It is clear from the figure that increasing the solidity and decreasing the tip speed is a relatively ineffective means of increasing the power loading as compared with decreasing the disk loading. The effect of rotor-blade average effective profile-drag coefficient is indicated by the tip-speed curve of 300 feet per second for $\delta = 0.006$ as compared with that for $\delta = 0.012$.

Rotor-speed-reduction gears.- The power required for hovering with a helicopter designed to operate at a maximum average lift-drag ratio in high speed can be reduced by the use of a rotor-speed-reduction gear. The high lift coefficients and corresponding high drag coefficients occurring at the tip of the retreating blade in high speed are absent in hovering. Maximum average lift-drag ratio of the blade sections occurs at a higher lift coefficient in hovering $(\mu = 0)$ than at high speed $(\mu = 0.3)$ with the result that a lower rotational speed is desirable in hovering. The optimum gear ratio and the resulting advantage depend on the characteristics of the airfoil sections used. In figure 22 the greatest percentage decrease in the power required for hovering, resulting from the use of a rotor-speed-reduction gear, is plotted against the equivalent rotor solidity for the three airfoil sections of figure 19. Calculations for the figure are explained in the appendix. The required gear ratios and maximum average lift-drag ratios are shown by the curves. It is observed that the power saving resulting from the use of a gear shift is greatly dependent upon the shape of the curve of airfoil section characteristics but tends to be largest for high-drag low-solidity blades.

CONCLUDING REMARKS

The relations among the primary aerodynamic variables affecting helicopter performance have been presented in the form of graphical charts. Trends in the variation of performance with the variation of primary variables can be obtained from the charts. Selected values of some of the variables, such as rotor-blade average effective profile-drag coefficient, tip-speed ratio, equivalent rotor solidity, and so forth, were used to cover a range of values expected to be encountered in present-day and future helicopters. For a given helicopter, those values are known and, therefore, the proper charts may be selected from which the correct performance trends may be obtained. If greater accuracy is desired, the construction of charts for exact values of the known variables is possible.

Langley Memorial Aeronautical Laboratory
National Advisory Committee for Aeronautics
Langley Field, Va., September 3, 1946

APPENDIX

METHODS FOR CONSTRUCTION OF CHARTS

The figures were constructed on the basis of the equations and charts of reference 1. Since helicopter performance depends upon many variables, some of these variables must be given representative fixed values in order to show performance trends in a graphical form. Each chart is made for certain fixed quantities, which are listed in the descriptions of the figures given in the present appendix. The construction of each figure for the present paper is described in sequence and many of the questions that arise in the analysis of the figures are thus clarified.

Figure 1.- Fixed quantities for figure 1 are as follows:

Altitude	Sea level
δ	0.012
σ	0.056
Y_t	320
R, ft	19
f, sq ft	10
b	3
V_h	0, 10, 20, 50, 75, 100, 150, 200

From the definitions of the parameters, it follows that when the value of $\frac{1}{F_h} = \frac{W}{P}\sqrt{\frac{W}{A}\frac{\rho_0}{\rho}}$ corresponding to a given value of $Y_h = V_h\sqrt{\frac{A}{W}\frac{\rho}{\rho_0}}$ is known, curves of constant horizontal velocity V_h may be plotted on scales of power loading W/P against disk loading W/A for any altitude for which the ratio ρ/ρ_0 is known. From equation (24) of reference 1

$$F_h = F_\delta + F_{f_h} + F_{i_h} + F_{rot} + F_b$$

The quantities that must be known to calculate each term are as follows:

Term	Quantity
F_δ	σ, δ, Y_h, Y_t
F_{f_h}	$C_{D_{f_h}}$, Y_h
F_{i_h}	Y_h
F_{rot}	F_{i_h}, Y_t
F_b	Y_h, b

It is thus seen that the six quantities needed to calculate F_h are σ, δ, Y_t, Y_h, $C_{D_{f_h}}$, and b. Five of these quantities (σ, δ, Y_t, Y_h, and b) are given directly by the stated conditions for figure 1. The value of $C_{D_{f_h}}$ is calculated from its definition

$$C_{D_{f_h}} = \frac{f_h}{A}$$

$$= \frac{10.0}{\pi 19^2}$$

$$= 0.00882$$

One curve of F_h against W/A can now be calculated from the charts of reference 1, and from this curve are obtained the constant-velocity curves of figure 1.

In a similar manner the hovering curve of figure 1 is plotted. From equation (45) of reference 1

$$F_v = F_\delta + F_{i_v} + F_{rot} + F_b$$

The power-loading parameter for hovering is considered a limiting case of that for vertical climb $\left(F_v \text{ with } Y_v \rightarrow 0\right)$. The quantities required to calculate F_v are σ, δ, Y_t, Y_v, and b. All are given by the stated conditions for the figure. For $Y_v = 0$, $F_{i_v} = 0.0264$ for uniform load distribution. The value of F_v is 0.0392, corresponding to which the hovering curve is drawn in figure 1.

Figure 2.- Figure 2 shows curves of maximum rate of climb superimposed for comparison on the hovering curve of figure 1. The necessary calculations are based on figure 6 of reference 1, which is reproduced herein as figure 10. The rate-of-forward-climb parameter Y_c is read from figure 10 for known values of Y and $F - F_h$. For the maximum rate of climb, use is made of the minimum value of F_h or F_{min} corresponding to a best value of Y_h or Y_{best} given by figure 7 of reference 1 in terms of σ, δ, Y_t, and $C_{D_{f_h}}$, all of which are known. In the present example, $F_{min} = 0.0235$ and the corresponding curve of W/P against W/A is plotted in figures 1 to 3 as the curve for $(W/P)_{max}$.

Figure 3.- Figure 3 shows curves of constant service ceiling $(60\ V_c = 100\ \text{ft/min})$ superimposed on the hovering and maximum power-loading curves from figure 1. These curves are based on the condition that the rotor driving power is proportional to the air density because of the engine characteristics. The development of the equation for the curves follows.

The quantities considered fixed for figure 3 are as follows:

σ	0.056
δ	0.012
Y_t	320
$C_{D_{f_h}}$	0.00882
b	3

The maximum rate of climb occurs for $Y = Y_{best}$. For the conditions at sea level $\left(\frac{\rho}{\rho_0} = 1\right)$ the value of Y_{best} obtained from figure 7 of reference 1 is 46.7 and does not change significantly with altitude. The power-loading parameter for the maximum

rate of climb is given by equation (48) of reference 1, which is approximately

$$Y_c = 550\left(F - F_{min}\right)$$

For the rate of climb of 100 feet per minute

$$Y_c = \frac{100}{60}\sqrt{\frac{A}{W}\frac{\rho}{\rho_0}}$$

and hence

$$\sqrt{\frac{A}{W}\frac{\rho}{\rho_0}} = 330\left(F - F_{min}\right) \tag{1}$$

At sea level $F_0 = \frac{P}{W}\sqrt{\frac{A}{W}}$ and at altitude $F_a = \frac{P}{W}\frac{\rho}{\rho_0}\sqrt{\frac{A}{W}\frac{\rho}{\rho_0}}$ if the rotor driving power is proportional to the density ratio. For $Y_{best} = 46.7$, the corresponding value of F (called F_{min}) is calculated from the sum

$$F_{min} = F_\delta + F_{f_h} + F_{i_h} + F_{rot} + F_b$$

as has been explained for F_h in connection with figure 1. The parameter that varies with altitude in the present example, namely, $Y_t = \Omega R\sqrt{\frac{A}{W}\frac{\rho}{\rho_0}}$, affects only the terms F and F_{rot}. The effect of Y_t on F_{rot} is negligible in comparison with F_{min}, and F_δ is then the only term causing an appreciable change in the value of F_{min} with altitude. In order to find F_δ, use is made of equation (23) of reference 1

$$F_\delta = \frac{\rho_0}{8} \frac{\sigma\delta}{550} \left(1 + 4.6\mu^2\right) Y_t^3$$

from which, for the specified constants,

$$F_\delta = 0.0130 \left[0.09 \sqrt{\frac{\rho}{\rho_0}} + 0.91 \left(\frac{\rho}{\rho_0}\right)^{3/2}\right]$$

At sea level, $F_{0_{min}} = 0.0235$ and, therefore, at altitude

$$F_{a_{min}} = 0.0235 + 0.0130 \left[0.09 \sqrt{\frac{\rho}{\rho_0}} + 0.91 \left(\frac{\rho}{\rho_0}\right)^{3/2}\right] - 0.0130$$

$$= 0.0105 + 0.0012 \sqrt{\frac{\rho}{\rho_0}} + 0.0118 \left(\frac{\rho}{\rho_0}\right)^{3/2}$$

Hence, from equation (1)

$$\sqrt{\frac{A}{W} \frac{\rho}{\rho_0}} = 330 \left(F_a - F_{a_{min}}\right)$$

$$= 330 \left[\frac{P}{W} \left(\frac{\rho}{\rho_0}\right)^{3/2} \sqrt{\frac{A}{W}} - 0.0105 - 0.0012 \sqrt{\frac{\rho}{\rho_0}} - 0.0118 \left(\frac{\rho}{\rho_0}\right)^{3/2}\right]$$

Solving for P/W gives

$$\frac{P}{W} = \frac{\rho_0}{330\rho} + \left[0.0105 \left(\frac{\rho_0}{\rho}\right)^{3/2} + 0.0012 \frac{\rho_0}{\rho} + 0.0118\right] \sqrt{\frac{W}{A}} \qquad (2)$$

Corresponding to each altitude is a ratio ρ/ρ_0, and from equation (2) is obtained a curve of W/P against W/A. Curves for standard density altitude are shown in figure 3.

Figure 4.- The quantities considered fixed in figure 4 are

σY_t^2	5740
μ	0.3
δ	0.012
$C_{D_{f_h}}$	0, 0.005, 0.01, 0.02, 0.03
b	3

As explained for figure 1, the six quantities needed to solve for F_h are σ, δ, Y_t, Y_h, $C_{D_{f_h}}$, and b. For each value of $C_{D_{f_h}}$ a curve of $1/F_h$ against Y_h or Y_t is defined by the constants for the figure. For example, a value of σ corresponds to each value of Y_t selected in accordance with the given condition $\sigma Y_t^2 = 5740$. (Graph of σ against $Y_t = \Omega R \sqrt{\frac{A}{W}\frac{\rho}{\rho_0}}$ is given in fig. 4.) Thus all quantities required for F_δ are known. Likewise, a value of Y_h corresponds to each value of Y_t in accordance with the relation $Y_h = \mu Y_t = 0.3\ Y_t$, thus all the quantities needed for F_h are known. In figure 4 the reciprocal of F_h, that is, $\frac{1}{F_h} = \frac{W}{P}\sqrt{\frac{W}{A}\frac{\rho_0}{\rho}}$, has been plotted to make the vertical scale proportional to the familiar quantity W/P.

Calculations for the hovering curves shown in figure 4 are similar to those explained in connection with figure 1. For each value of Y_t selected, σ is obtained, as in the case of horizontal flight, from the relation $\sigma Y_t^2 = 5740$. Calculations of F_δ were made for both $\delta = 0.012$ and $\delta = 0.006$; thus, the two hovering curves shown in figure 4 are produced.

As explained for figure 1, the value of the induced power-loading parameter in vertical flight F_{i_v} needed to calculate F applies to hovering when $Y_v \longrightarrow 0$. The value of F_{i_v} varies with the blade shape, the lowest value occurring with blades shaped for uniform axial-inflow-velocity distribution. Such distributions

require a tapered and/or twisted blade. For untwisted rectangular blades the value of F_{i_v} is approximately 6 percent higher. In the present calculation the minimum value of $F_{i_v} = 0.0264$ is generally used because it serves as a convenient reference. The hovering curve in figure 1 shows only about 4 percent difference in W/P for the two extreme cases.

Figure 5.- Figure 5 is similar to figure 4 except that δ has a value of 0.006 instead of 0.012.

Figure 6.- Figure 6 is similar to figure 4 except the quantity μ is the variable rather than Y_h, which is fixed at 75. Curves of constant $\delta = 0.012$ and $\delta = 0.006$ are shown for $C_{D_{f_h}} = 0.010$.

Figures 7 and 8.- The calculations made for figures 7 and 8 are similar to those made for figure 2.

Figure 9.- Figure 9 includes, in addition to the hovering curve for $\delta = 0.012$ of figure 4, curves for vertical flight for two values of $C_{D_{f_v}}$ and for values of the rate-of-vertical-climb parameter up to $Y_v = 30$. The calculations for this figure differ from those for hovering only in obtaining F_{i_v} for the given values of $C_{D_{f_v}}$ and Y_v from figure 5 of reference 1.

Figure 10.- Figure 10 is a reproduction of figure 6 of reference 1.

Figure 11.- Figure 11 differs from the generalized figure 4 in substitution of constant f/P for $C_{D_{f_h}}$ and in selection of the values $\sigma = 0.056$, $Y_t = 320$, $Y_h = 96$, and $\frac{\rho}{\rho_0} = 1$.

By definition,

$$C_{D_{f_h}} = \frac{f_h}{A}$$

$$= \frac{f_h}{P}\frac{P}{W}\sqrt{\frac{A}{W}\frac{\rho}{\rho_0}}\left(\frac{W}{A}\right)^{3/2}\sqrt{\frac{\rho_0}{\rho}}$$

$$= \frac{f_h}{P}F_h\sqrt{\frac{W}{A}\frac{\rho_0}{\rho}}\frac{W}{A}$$

For $\frac{\rho}{\rho_0} = 1$

$$C_{D_{f_h}} = \frac{f_h}{P} F_h \left(\frac{W}{A}\right)^{3/2} \tag{3}$$

By means of equation (3), points in figure 11 may be calculated from points on the ordinate $Y_t = 320$ of figure 4.

Calculations for the curves of constant rate of climb are similar to those for figure 2. The necessary quantities σ, δ, and Y_t are all known, and to each set of values of W/P, W/A, and f_h/P there corresponds a value of $C_{D_{f_h}}$ in accordance with equation (3).

The boundary of the region of stall is calculated on the basis of figure 8 of reference 1. The figure shows that for the assumed value of $\sigma Y_t^2 = 5740$, stalling of the blade tips may be expected when the value of the quantity λ/μ is near 0.5 for $\mu = 0.3$ with μ corresponding to a section lift coefficient of approximately 1.5. From the lower part of the same figure it is seen that with $Y_h = 96$ the value of $C_{D_{f_h}}$ is about 0.03. By means of this value and of equation (3), the stalling region is defined in figure 11.

Figures 12 to 16.- Figures 12 to 16 are constructed similarly to figure 11 but with different fixed values of δ or μ.

Figure 17.- The condition that the helicopter shall fly at its maximum speed with the same power as required for hovering restricts solutions to the points of intersection of curves of constant $C_{D_{f_h}}$ with the hovering curve in figure 4. From these intersections the curves of constant f_h/P of figure 17 are obtained by use of the relation between $C_{D_{f_h}}$ and f_h/P (equation (3)), which was derived for figure 11, and by use of the hovering curve of figure 4 for uniform disk loading with $\delta = 0.012$. The intersections in figure 4 also determine values of Y_h and, therefore, curves of constant V_h, which are also curves of constant ΩR in figure 17 because μ is constant. The curves of

constant f/P are found to be nearly coincident with the curves of constant V_h or of constant ΩR. Curves of constant service ceiling were calculated by the method described for figure 3, the proper values of the constant quantities being used.

Figure 18.- The calculations for the curves of figure 18 are explained for figure 17, except that the curves for constant rate of climb are obtained by calculations of the type described for figure 2 but with the appropriate constants.

Figure 19.- Figure 19 is adapted from figure 1 of reference 3.

Figure 20.- By reduction in the gross weight of a hovering helicopter, power may be made available for a rate of vertical climb. For the hovering condition, F_{i_v} has a value of 0.0264. From the definition

$$F_{i_v} = \frac{P_{i_v}}{W} \sqrt{\frac{A}{W} \frac{\rho}{\rho_0}}$$

$$\approx \frac{1}{W^{3/2}}$$

it follows that if the gross weight W is reduced by ΔW then

$$F_{i_v} = \frac{0.0264}{\left(1 - \frac{\Delta W}{W}\right)^{3/2}}$$

By means of figure 5 of reference 1, values of Y_v may be read for known values of F_{i_v} and $C_{D_{f_v}}$ on the assumption that the power absorbed in blade profile drag does not vary with rate of vertical climb. These quantities define curves of constant W/A and constant $C_{D_{f_v}}$ on coordinates of V_v against $\Delta W/W$.

Figure 21.- Curves of constant tip speed ΩR on coordinates of W/P against W/A are plotted in figure 21 from the generalized

hovering curve of figure 4 for uniform disk loading. For the condition $\sigma Y_t^2 = 5740$, the curves of constant σ are similarly obtained.

Figure 22.- In the construction of figure 22 arbitrary values of σY_t^2 are selected. The corresponding values of δ are calculated by the method of reference 1 for one of the curves in figure 19. By this method the value of δ is the constant drag coefficient that would absorb the same power as the drag coefficient which varies in accordance with the curves of airfoil section characteristics. Then, from a plot of $\sigma\delta Y_t^2$ against σY_t^2 the coordinates of the minimum are read. The values of δ and of σY_t^2 are thus determined for maximum average lift-drag ratio. This procedure is carried out for hovering $(\mu = 0)$ and for high speed $(\mu = 0.3)$. For fixed values of σ the ratio of the tip-speed parameters is the required gear ratio. The values of δ and σY_t^2 thus obtained for hovering, when used to calculate the value of F_v for any selected value of σ, may be considered to give the hovering performance when a rotor-speed-reduction gear is employed. In order to find the performance when a gear is not used, the value of δ is calculated for hovering, the optimum value of σY_t^2 for high speed being used. The ratio of the power-loading parameters for vertical flight represents the ratio of the power required for hovering with and without the gear.

REFERENCES

1. Talkin, Herbert W.: Charts for Helicopter-Performance Estimation. NACA ACR No. L5E04, 1945.

2. Gustafson, F. B., and Gessow, Alfred: Effect of Rotor-Tip Speed on Helicopter Hovering Performance and Maximum Forward Speed. NACA ARR No. L6A16, 1946.

3. Gustafson, F. B.: Effect on Helicopter Performance of Modifications in Profile-Drag Characteristics of Rotor-Blade Airfoil Sections. NACA ACR No. L4H05, 1944.

TABLE I

SUMMARY OF CHARTS

Condition	Figure
Generalized charts	
Horizontal flight and hovering	4 to 6
Vertical climb and hovering	9
Rate of climb and ceiling	7, 8, 10
Power-loading disk-loading charts	
Horizontal flight, climb, and hovering	11 to 16
Vertical climb and hovering	21
Helicopters that will hover	17, 18
Special-purpose charts	
Vertical climb by means of weight reduction	20
Effect of rotor-speed-reduction gears on hovering	22

NATIONAL ADVISORY
COMMITTEE FOR AERONAUTICS

TABLE II

ELEMENTARY DESIGN VARIABLES

Definition	Symbol
Rotor-disk area	A
Fuselage equivalent flat-plate area	f
Rotor power	P
Gross weight of helicopter minus fuselage lift	W
Equivalent rotor solidity	σ
Mass density of air	ρ
Rotor angular velocity	Ω

TABLE III

ELEMENTARY PERFORMANCE VARIABLES

Definition	Symbol
Maximum rate of climb in forward flight	V_c
Maximum horizontal velocity	V_h
Rate of vertical climb (for hovering, $V_v = 0$)	V_v
Ceiling (expressed in terms of density ratio)	ρ/ρ_0

NATIONAL ADVISORY
COMMITTEE FOR AERONAUTICS

TABLE IV

FUNDAMENTAL DESIGN PARAMETERS

Definition	Symbol	Formula
Power-loading parameter	F	$\frac{P}{W}\sqrt{\frac{A}{W}\frac{\rho}{\rho_0}}$
Tip-speed parameter	Y_t	$\Omega R\sqrt{\frac{A}{W}\frac{\rho}{\rho_0}}$
Helicopter drag coefficient based on rotor-disk area	C_{D_f}	f/A
Equivalent rotor solidity	σ	$\frac{4b}{\pi R}\int_0^1 x^3 c_x\,dx$

TABLE V

FUNDAMENTAL PERFORMANCE PARAMETERS

Definition	Symbol	Formula
Maximum velocity parameter	Y	$V\sqrt{\frac{A}{W}\frac{\rho}{\rho_0}}$
Maximum rate-of-forward-climb parameter	Y_c	$V_c\sqrt{\frac{A}{W}\frac{\rho}{\rho_0}}$
Rate-of-vertical-climb parameter	Y_v	$V_v\sqrt{\frac{A}{W}\frac{\rho}{\rho_0}}$
Horizontal-velocity parameter	Y_h	$V_h\sqrt{\frac{A}{W}\frac{\rho}{\rho_0}}$

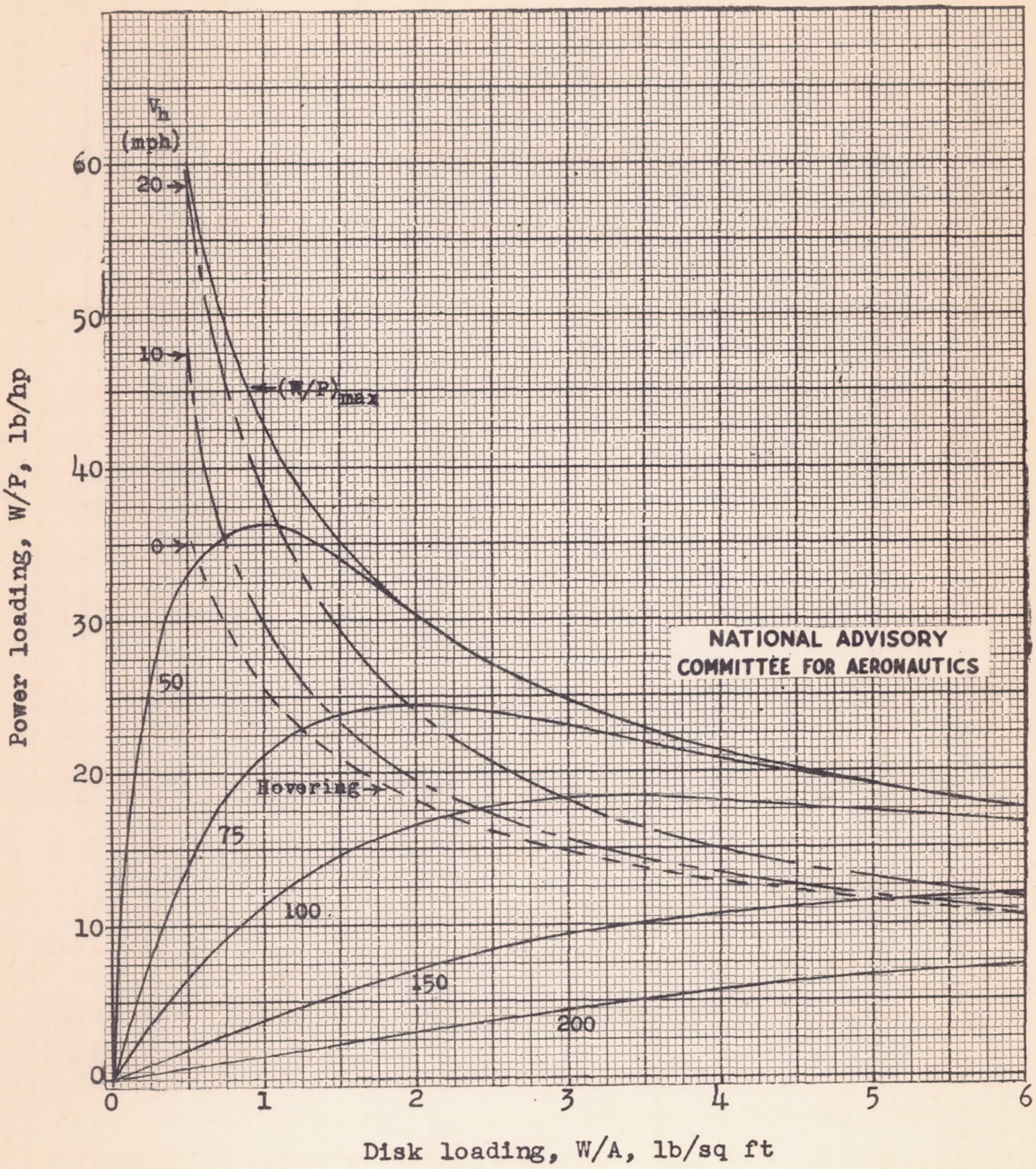

Figure 1.- Specialized selection chart for horizontal flight and hovering. ρ = 0.002378 slug per cubic foot; δ = 0.012; σ = 0.056; Y_t = 320; R = 19.0 feet; f = 10.0 square feet.

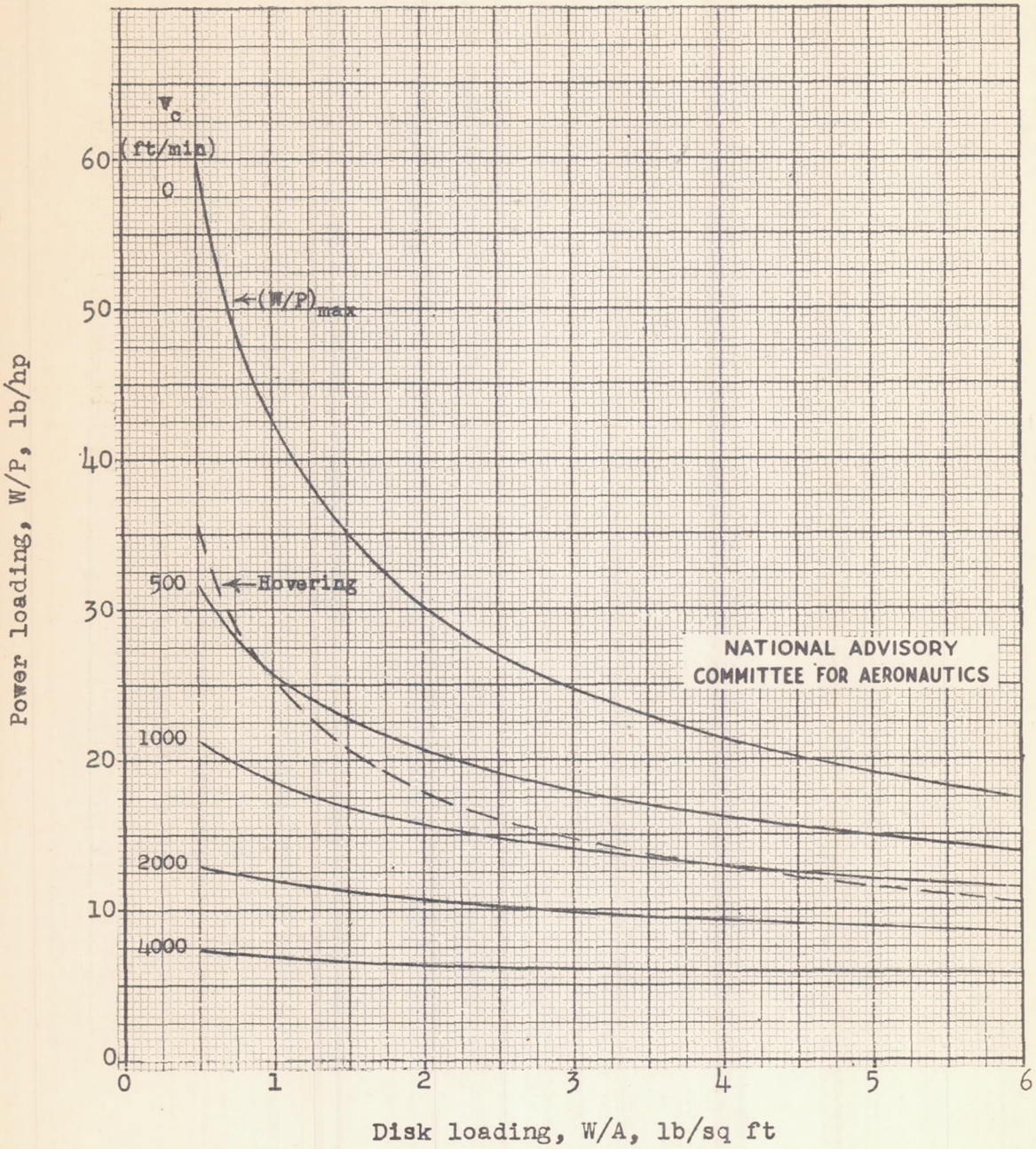

Figure 2.- Maximum rate of climb for the conditions of figure 1.

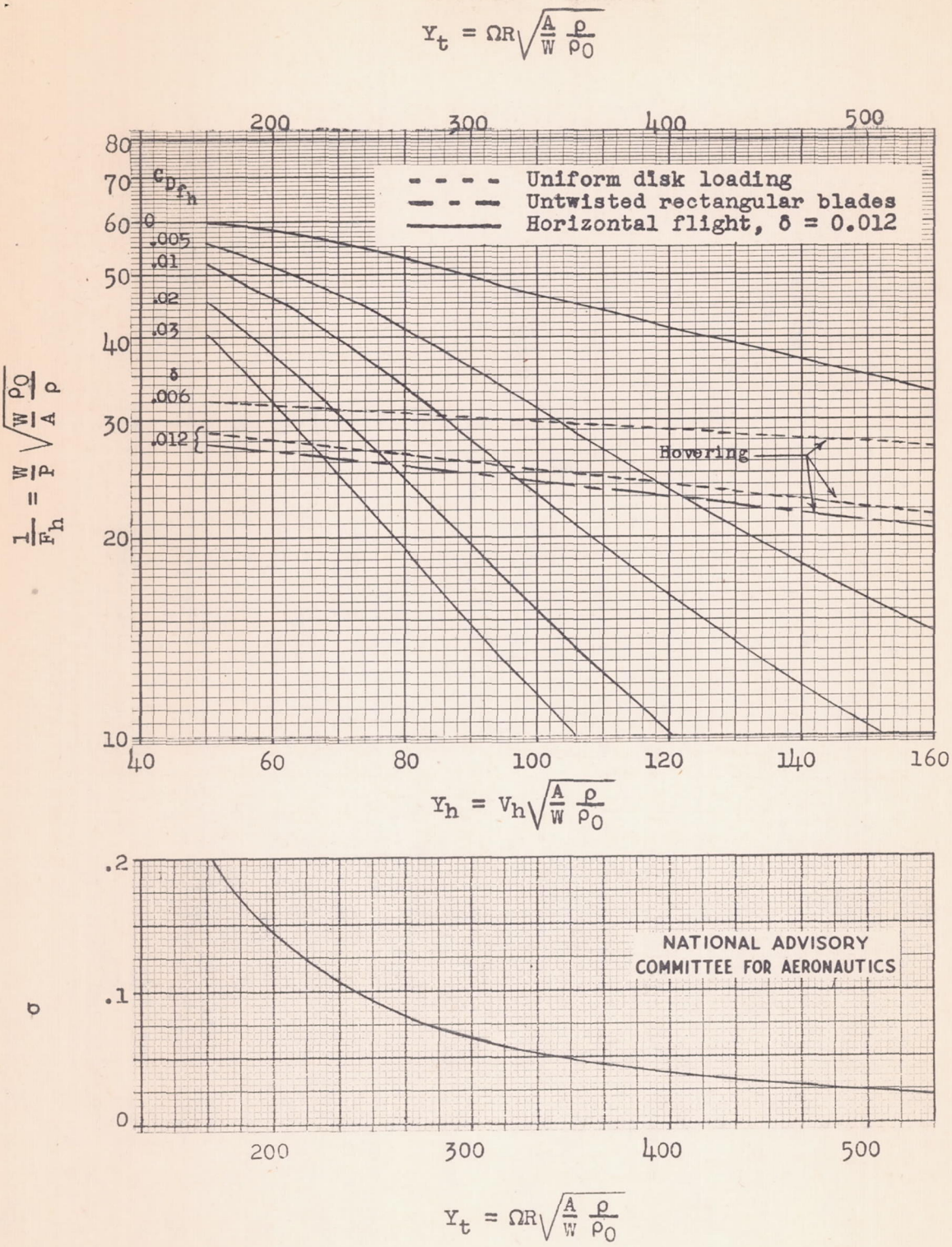

Figure 4.- Generalized performance chart for horizontal flight and hovering. $\mu = 0.3$; $\delta = 0.012$; $\sigma Y_t^2 = 5740$.

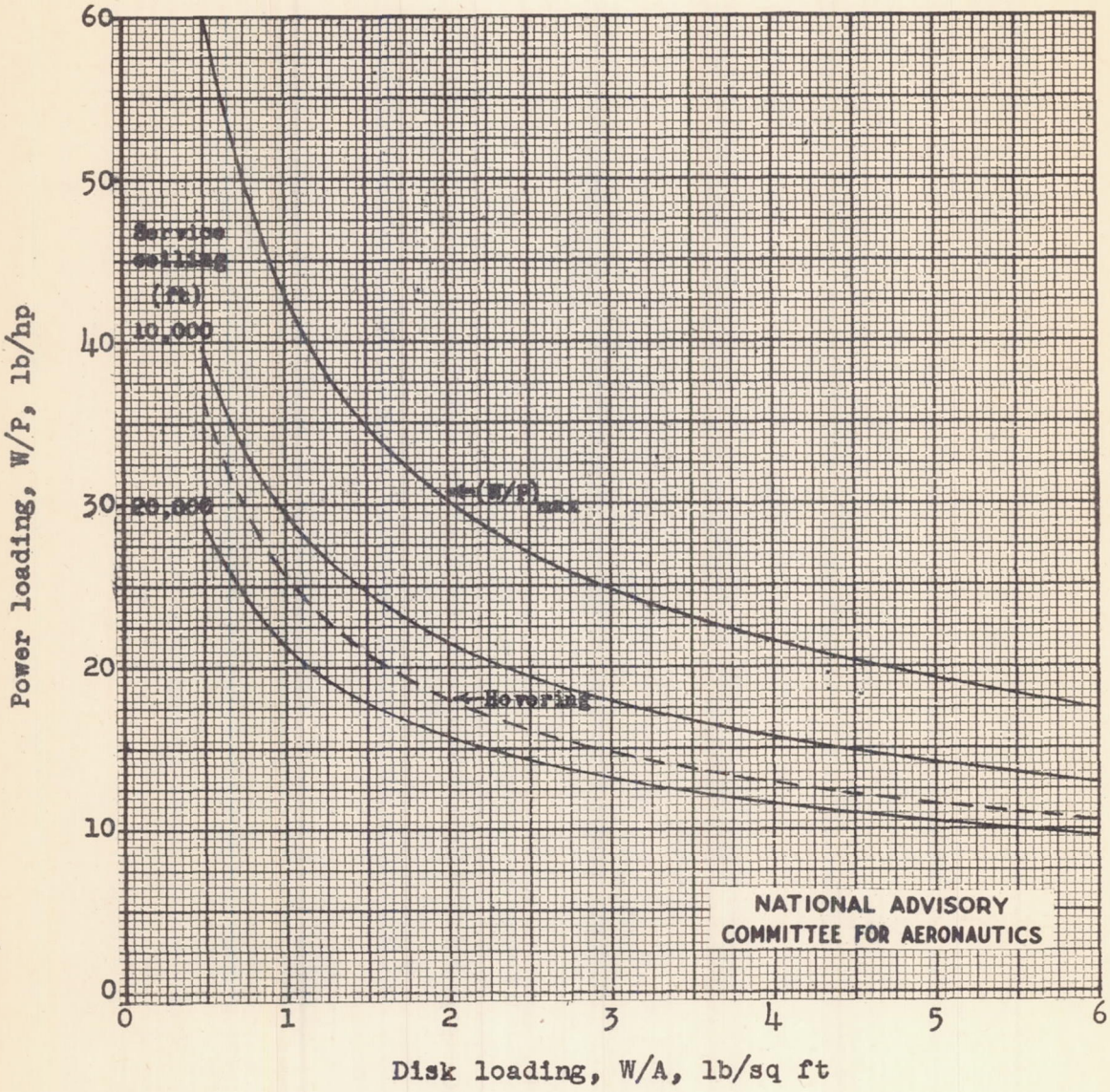

Figure 3.- Service ceiling for the conditions of figure 1.

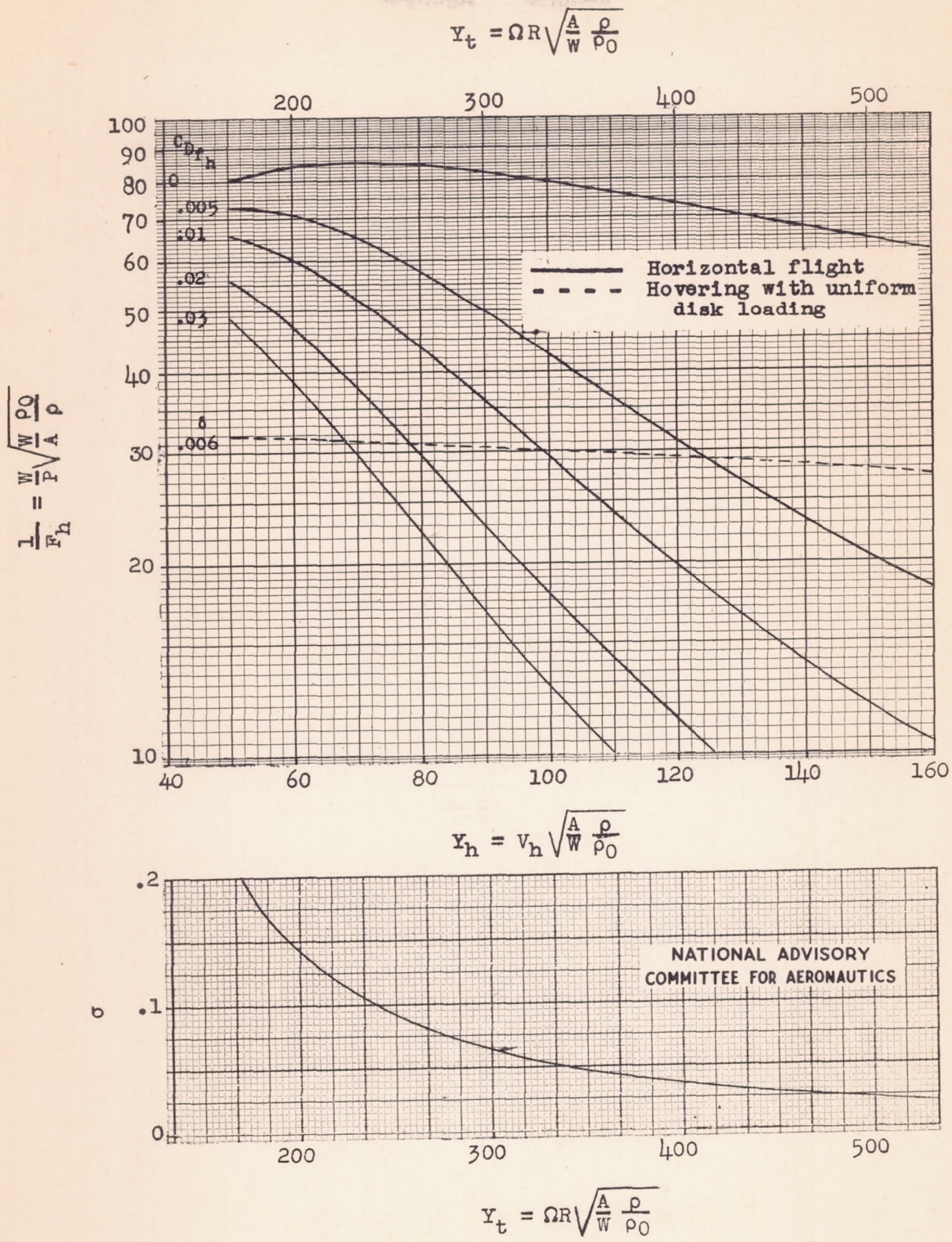

Figure 5.- Generalized performance chart for horizontal flight and hovering. $\mu = 0.3$; $\delta = 0.006$; $\sigma Y_t^2 = 5740$.

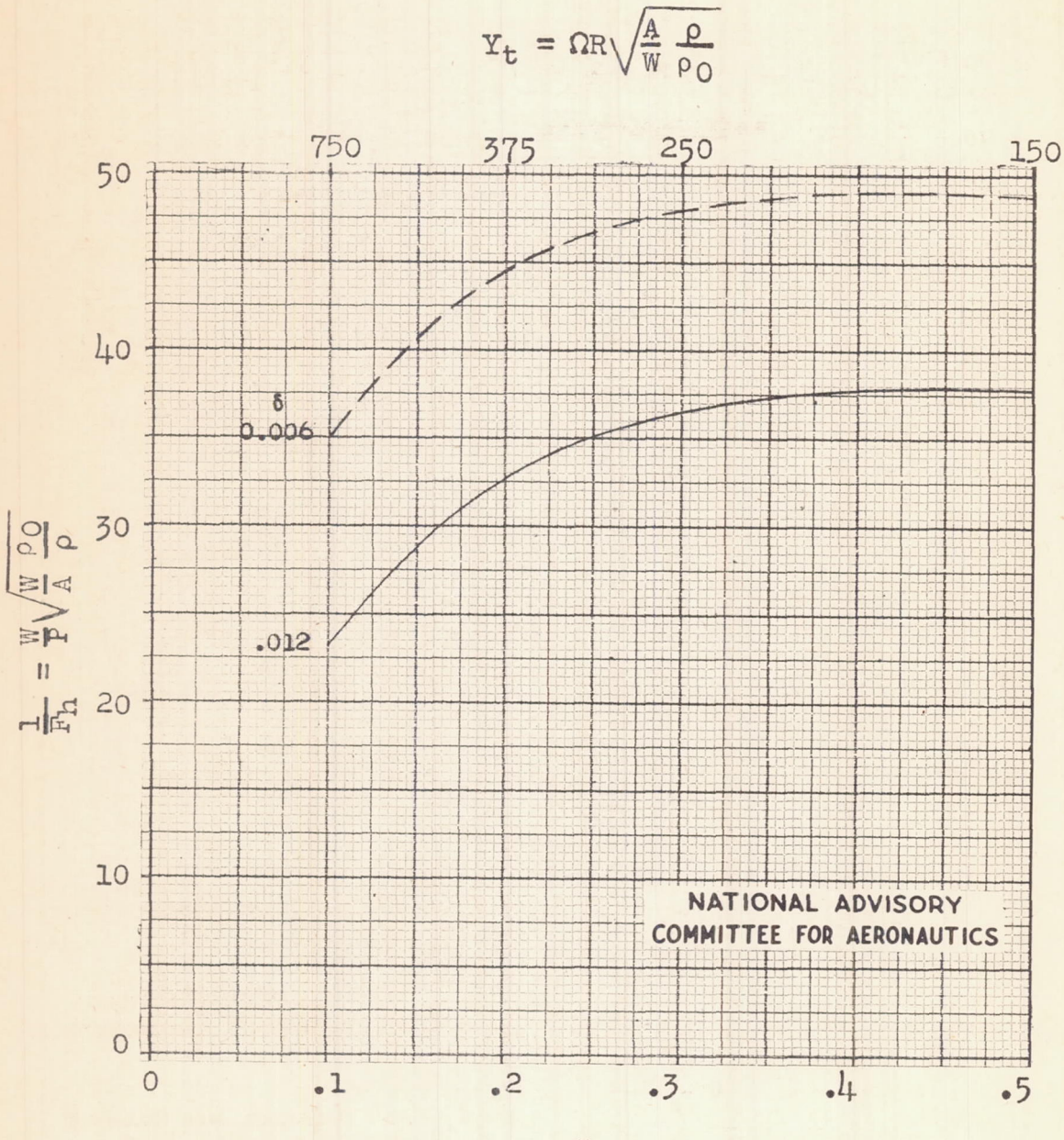

Figure 6.- Variation of $\frac{1}{F_h}$ with μ. $\sigma Y_t^2 = 5740$; $Y_h = 75$; $C_{D_{f_h}} = 0.01$.

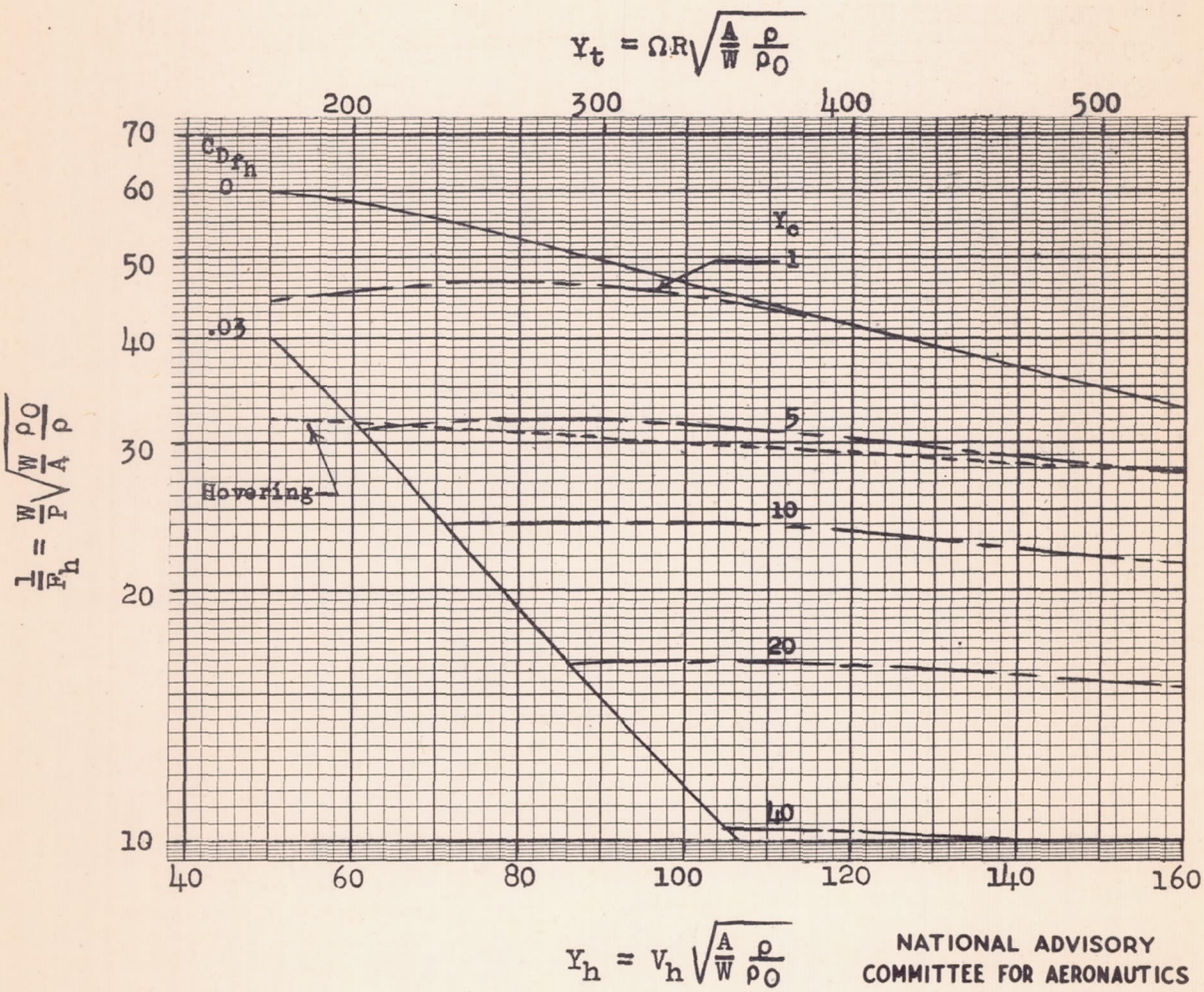

Figure 7.- Generalized performance chart for maximum rate of climb for the conditions of figure 4. $\delta = 0.012$. (V_h is the maximum speed, i.e. for $Y_c = 0$.)

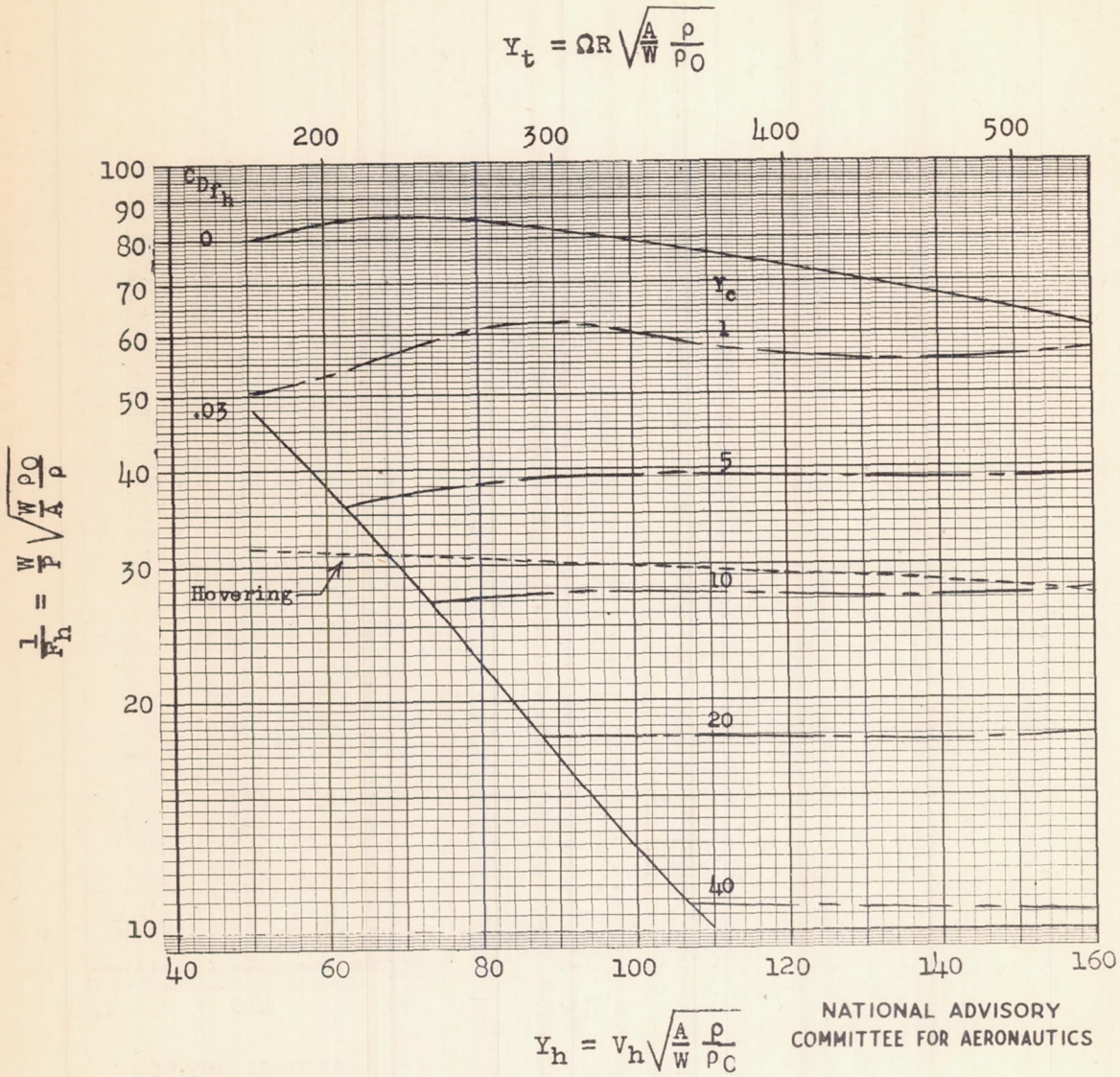

Figure 8.- Generalized performance chart for maximum rate of climb for the conditions of figure 5. $\delta = 0.006$. (V_h is the maximum speed, i.e. for $Y_c = 0$.)

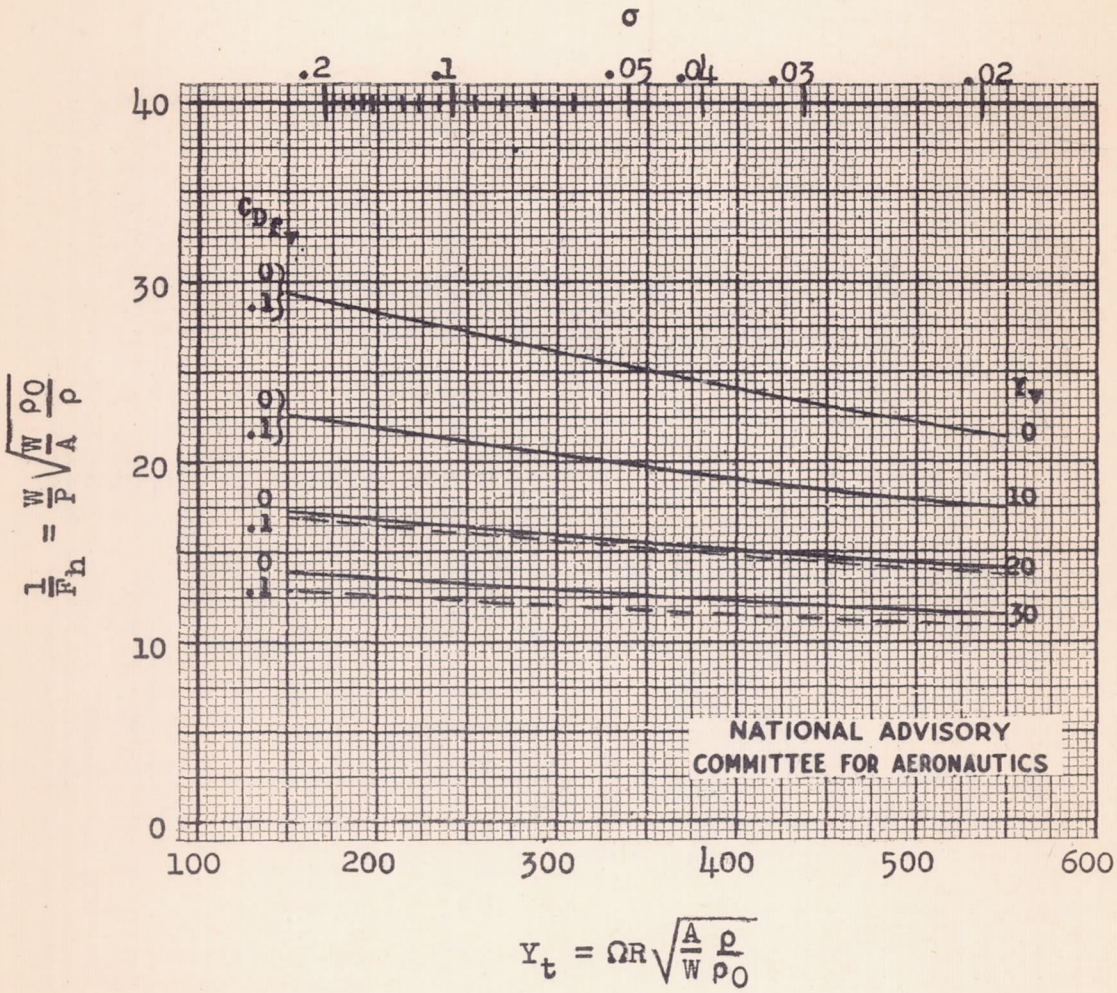

Figure 9.- Generalized performance chart for constant values of the rate-of-vertical-climb parameter Y_v at sea level. $\delta = 0.012$; $\sigma Y_t^2 = 5740$.

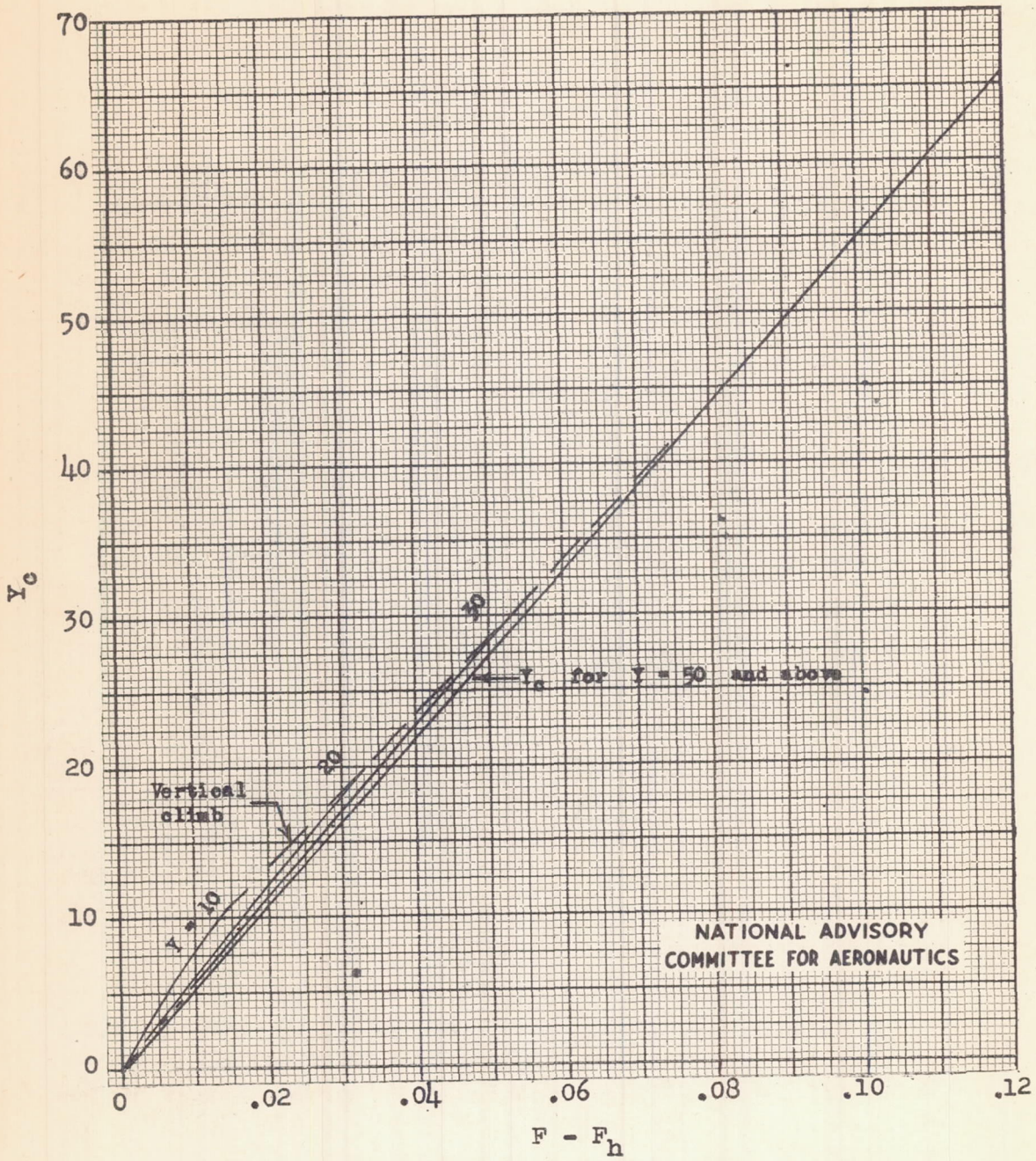

Figure 10.- Chart for finding the rate-of-forward-climb parameter Y_c.

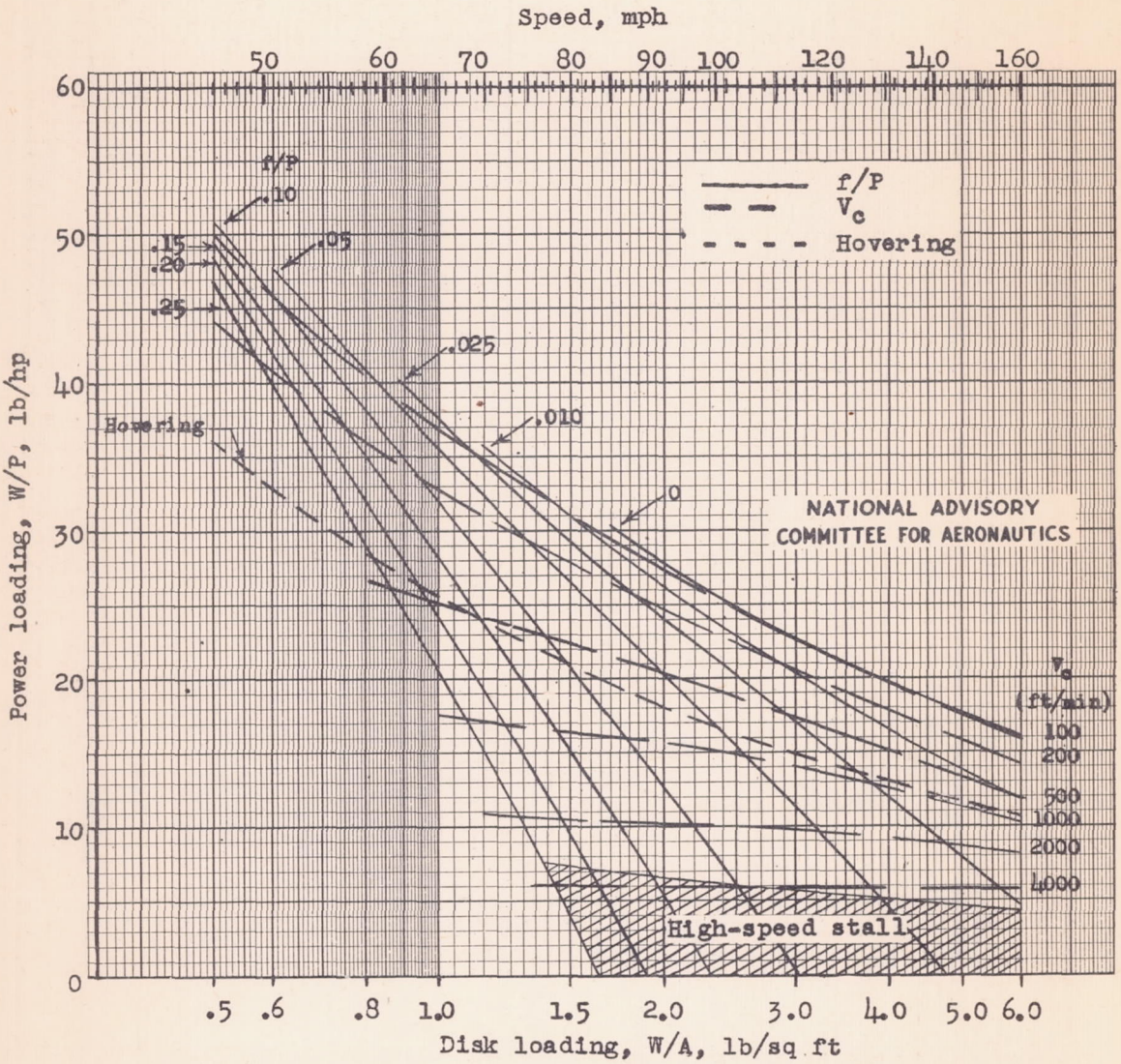

Figure 11.- Power-loading disk-loading performance chart for sea level. $\mu = 0.3$; $\delta = 0.012$; $\sigma = 0.056$; $\sigma Y_t^2 = 5740$.

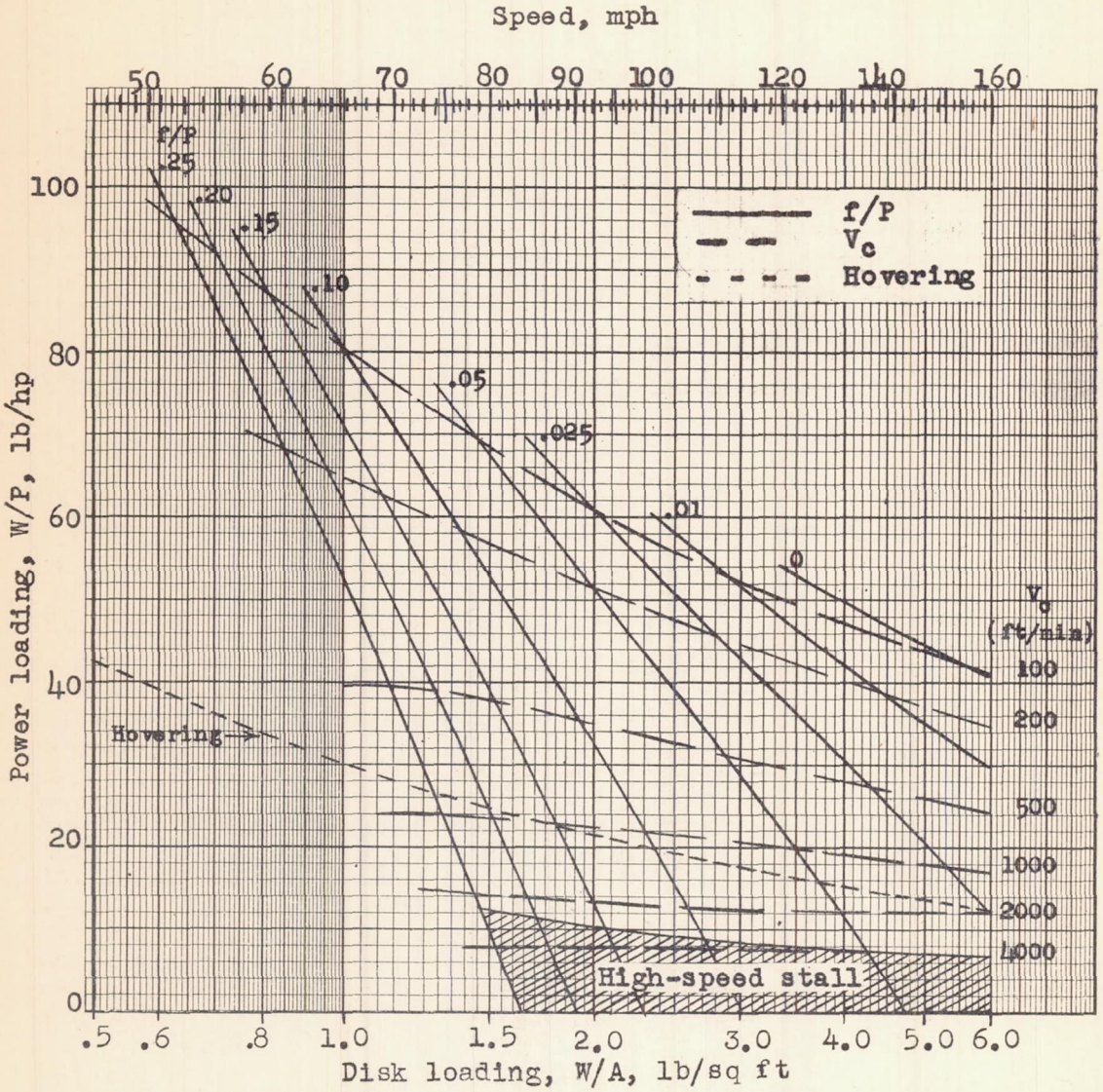

Figure 12.- Power-loading disk-loading performance chart for sea level. $\mu = 0.3$; $\delta = 0.006$; $\sigma = 0.056$; $\sigma Y_t^2 = 5740$.

NATIONAL ADVISORY
COMMITTEE FOR AERONAUTICS

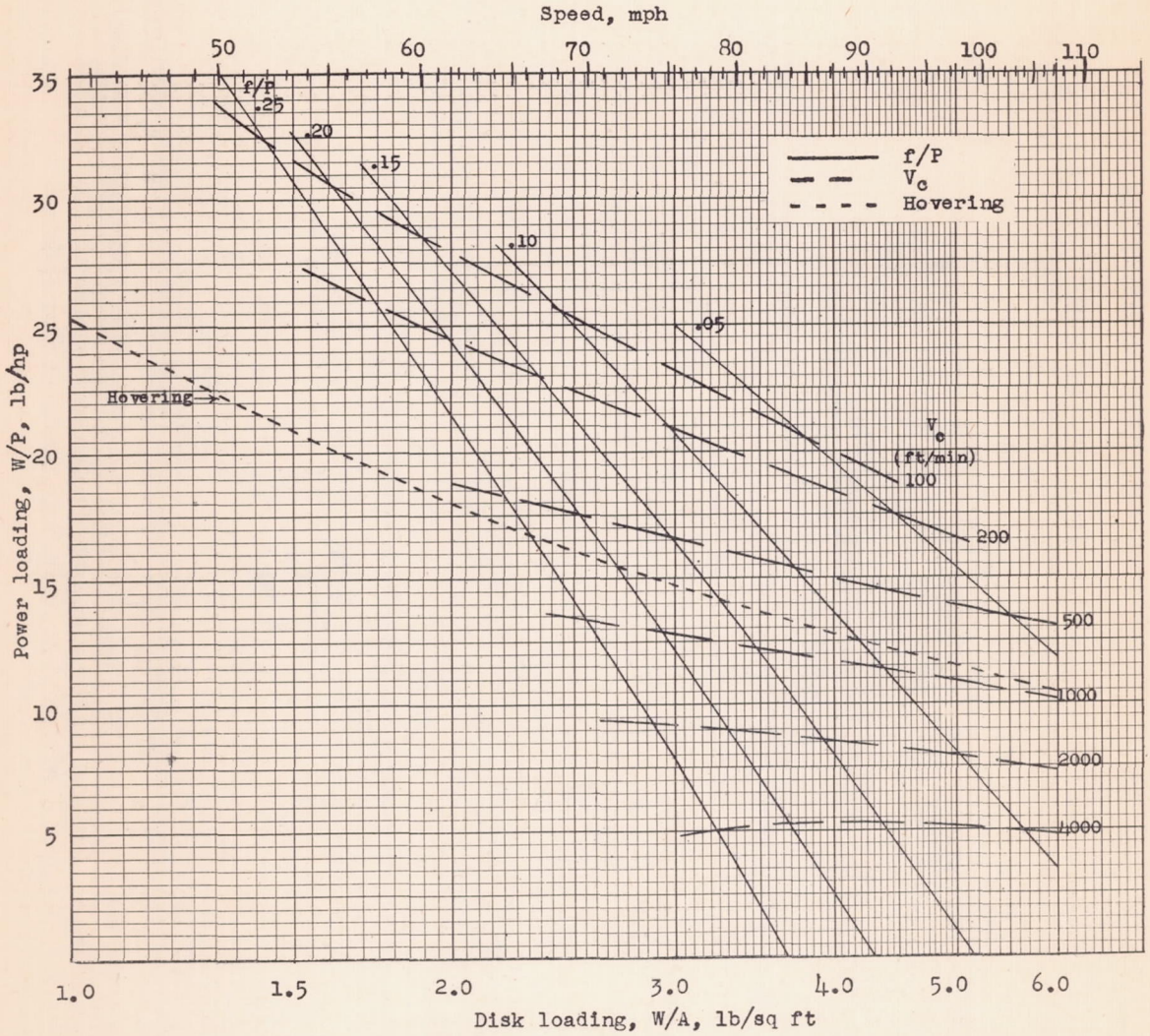

Figure 13.- Power-loading disk-loading performance chart for sea level. $\mu = 0.2$; $\delta = 0.012$; $\sigma = 0.056$; $\sigma Y_t^2 = 5740$.

NATIONAL ADVISORY
COMMITTEE FOR AERONAUTICS

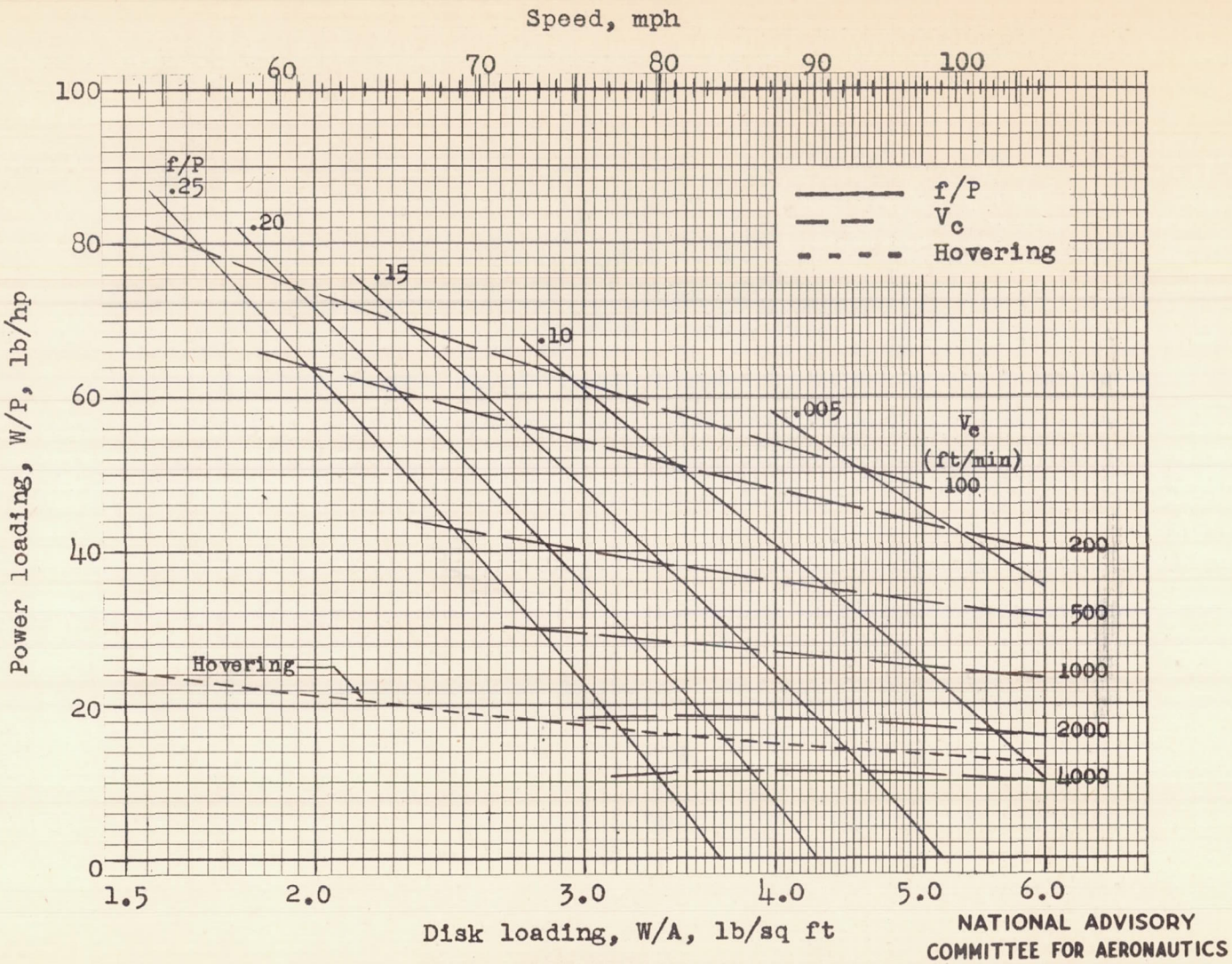

Figure 14.- Power-loading disk-loading performance chart for sea level. $\mu = 0.2$; $\delta = 0.006$; $\sigma = 0.056$; $\sigma Y_t^2 = 5740$.

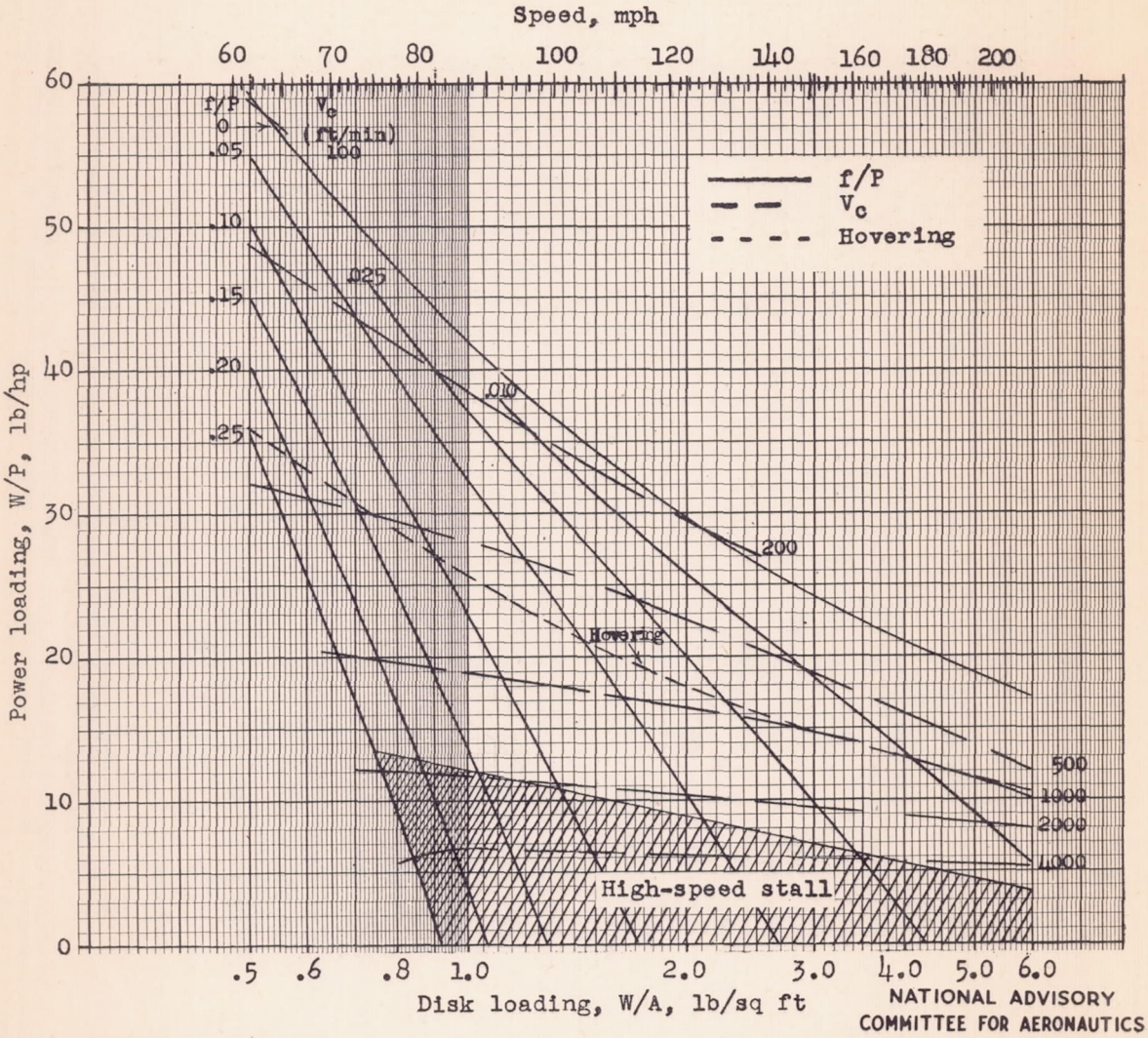

Figure 15.- Power-loading disk-loading performance chart for sea level. $\mu = 0.4$; $\delta = 0.012$; $\sigma = 0.056$; $\sigma Y_t^2 = 5740$.

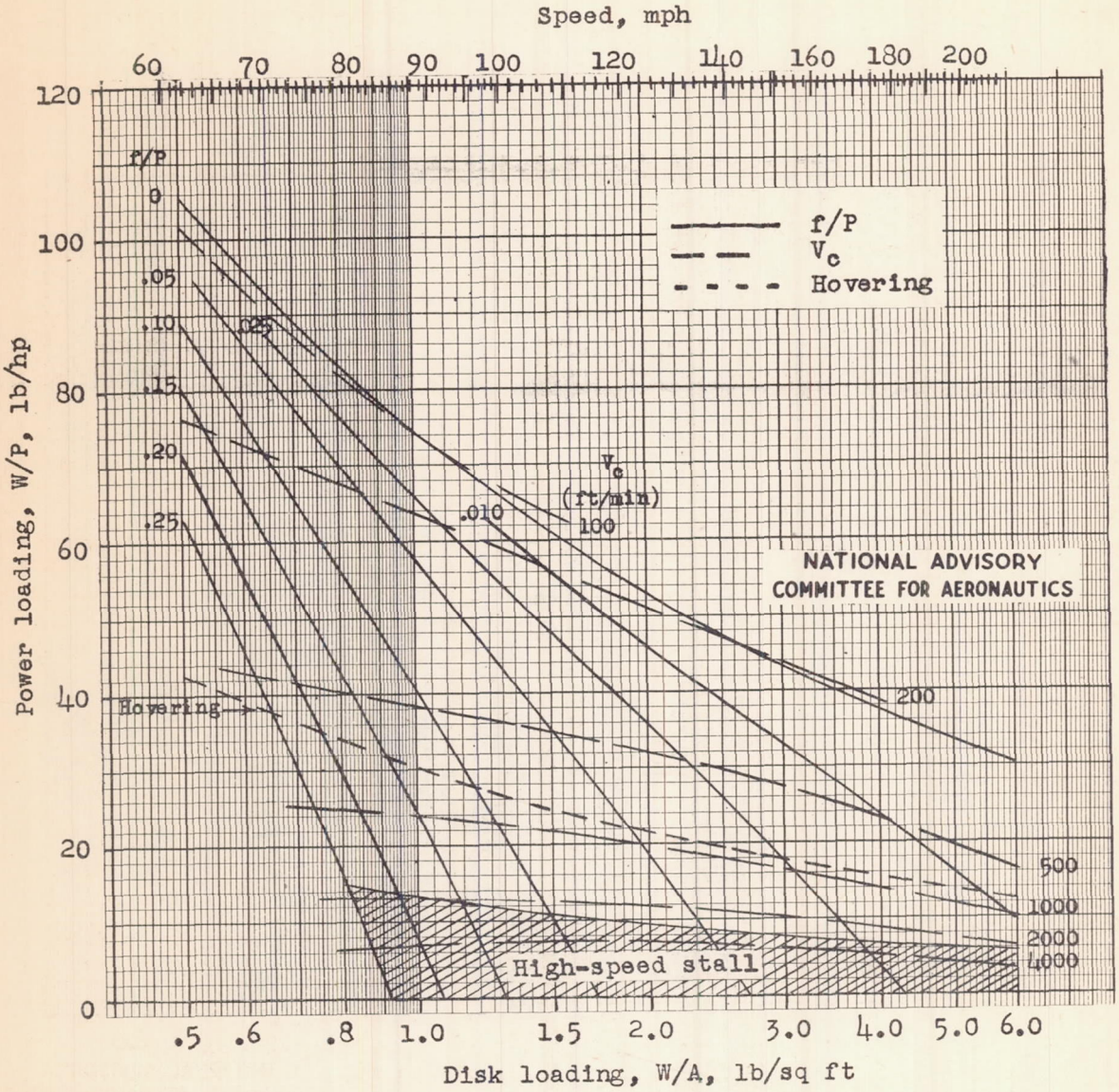

Figure 16.- Power-loading disk-loading performance chart for sea level. $\mu = 0.4$; $\delta = 0.006$; $\sigma = 0.056$; $\sigma Y_t^2 = 5740$.

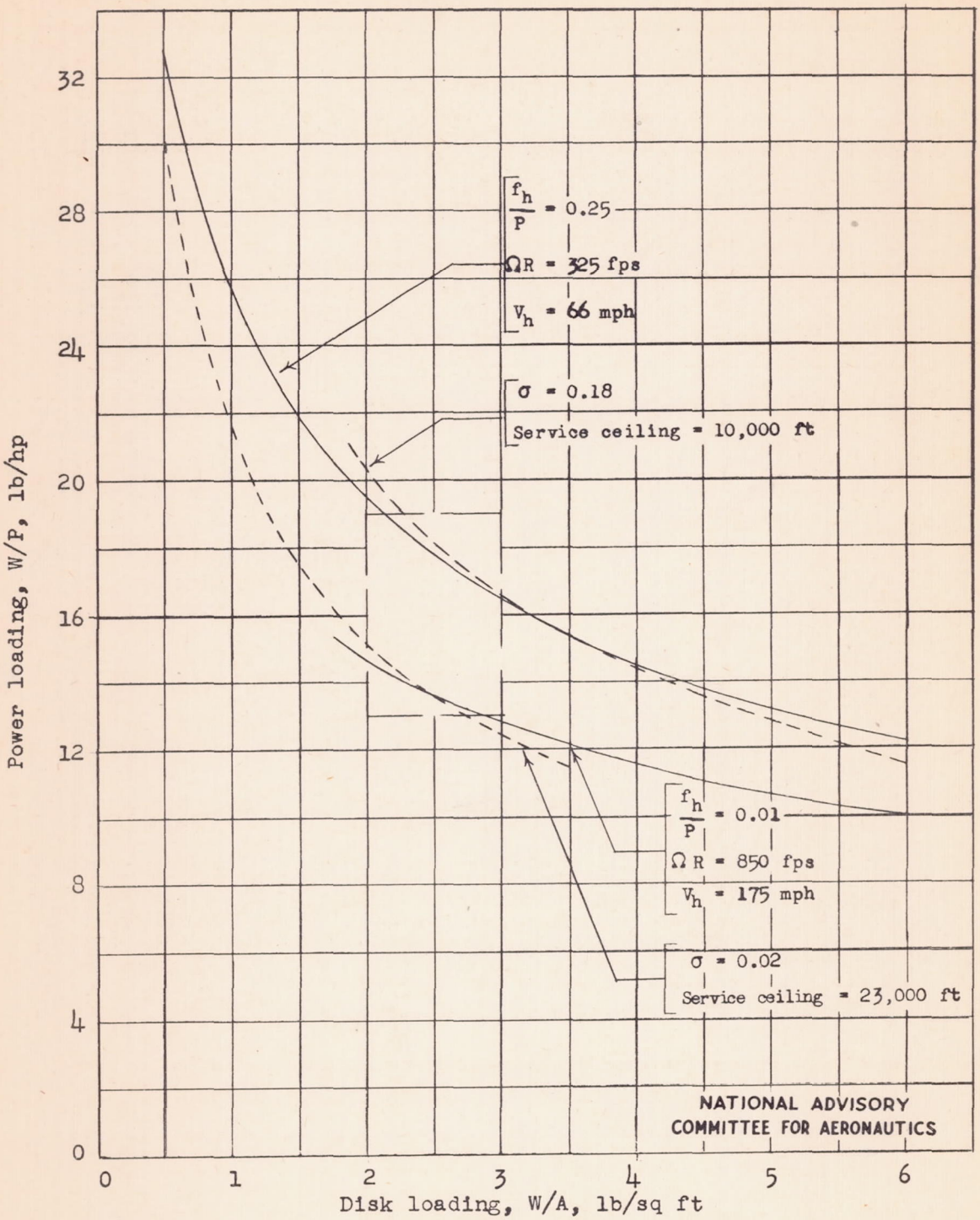

Figure 17.- Power-loading disk-loading performance chart for sea level for helicopters with power just sufficient to hover. $\mu = 0.3$; $\delta = 0.012$; $\sigma Y_t^2 = 5740$.

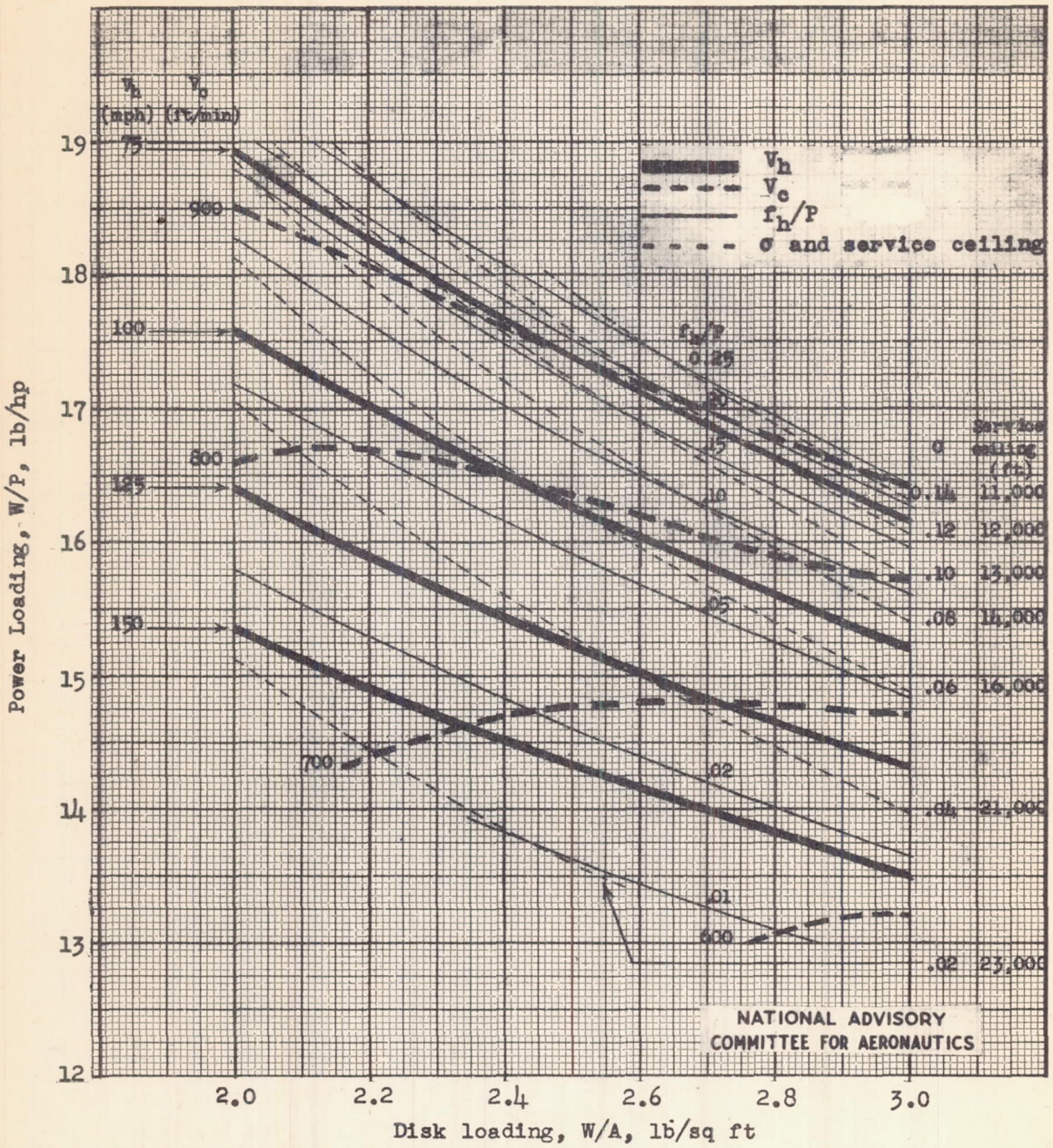

Figure 18.- Enlarged power-loading disk-loading performance chart for sea level for helicopters with power just sufficient to hover. $\mu = 0.3$; $\delta = 0.012$; $\sigma Y_t^2 = 5740$.

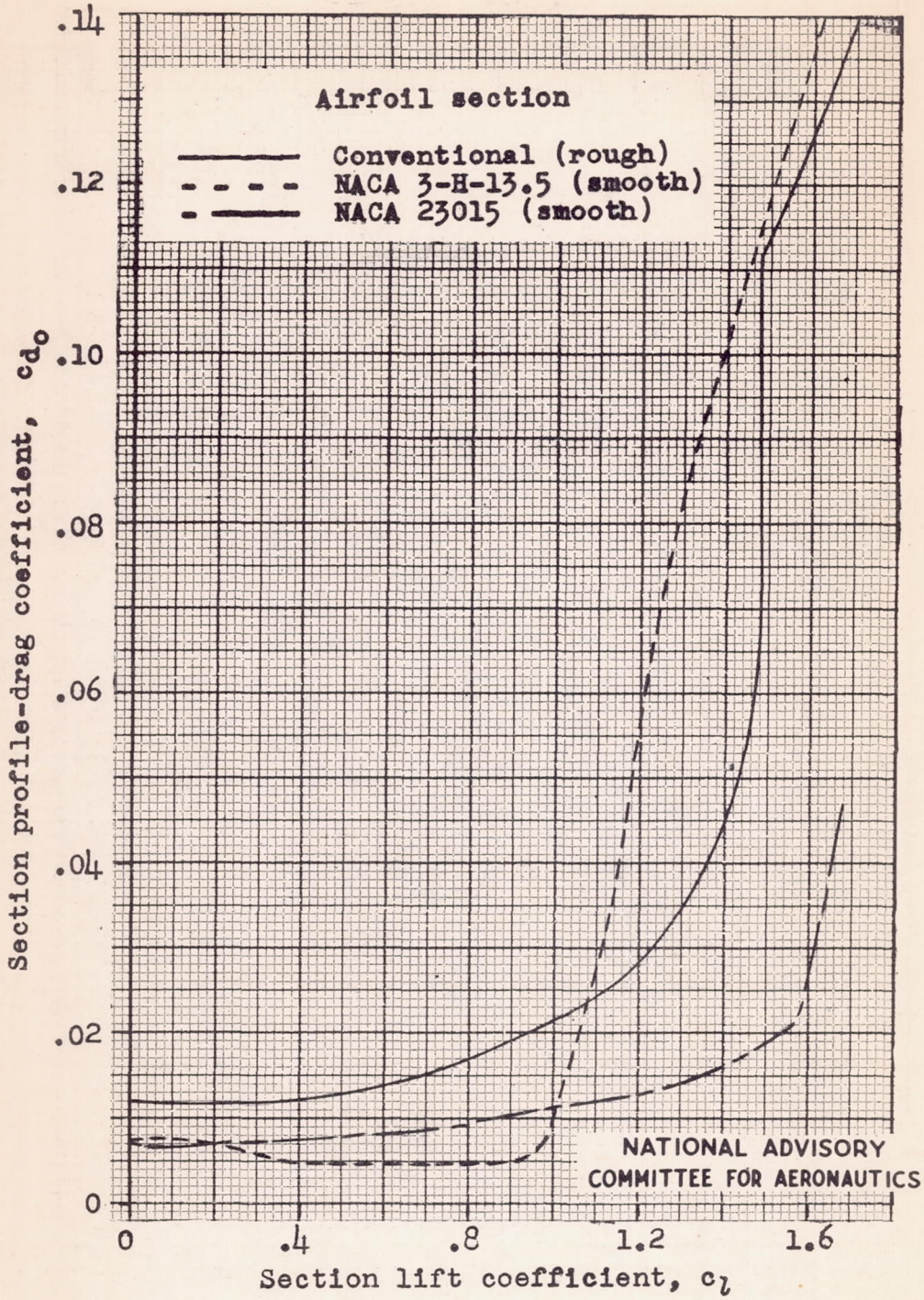

Figure 19.- Airfoil section profile-drag coefficient c_{d_o} against section lift coefficient c_l for the airfoil sections of figure 1 from reference 3.

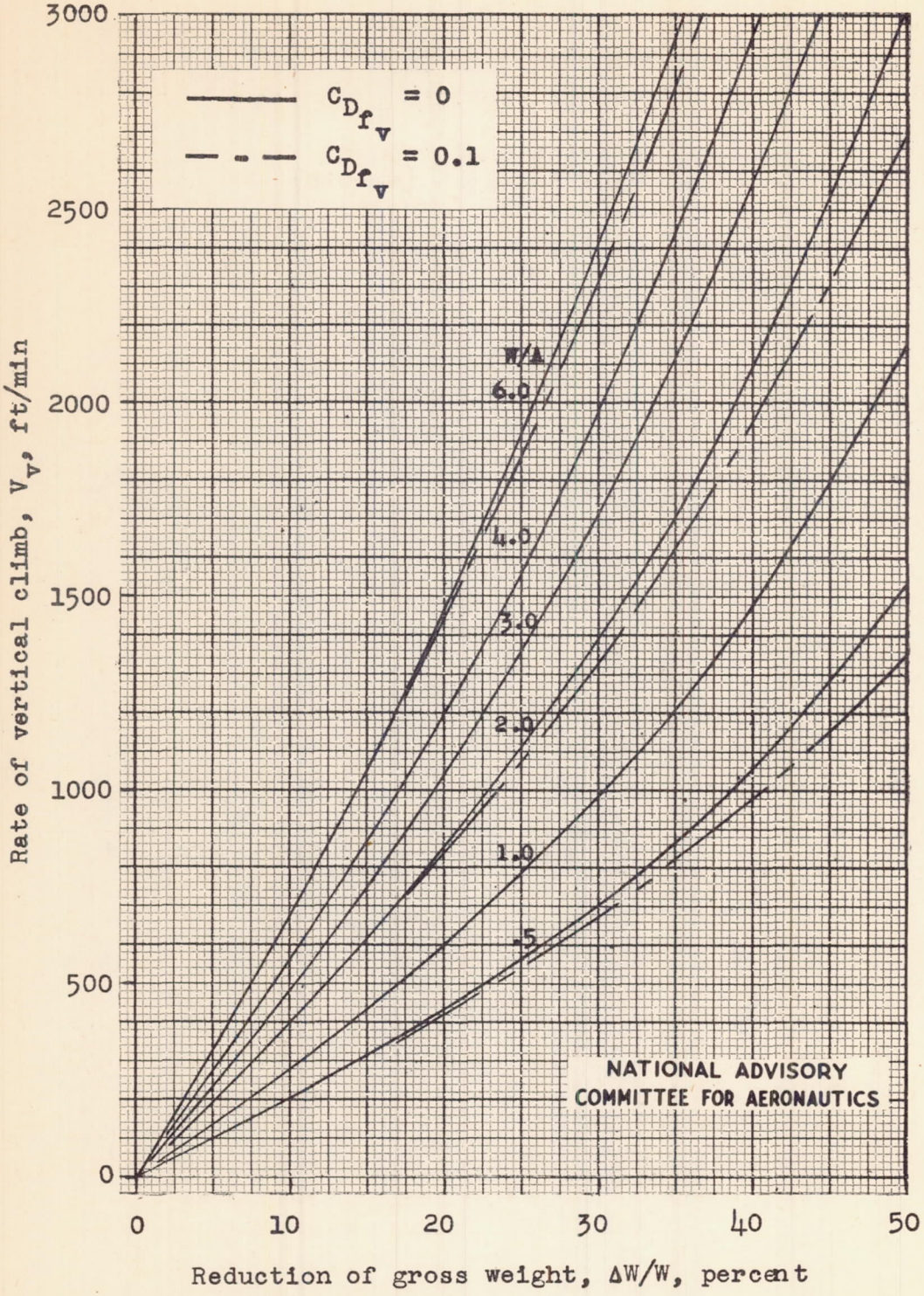

Figure 20.- Rate of vertical climb obtainable by reduction in gross weight of helicopters with power just sufficient to hover.

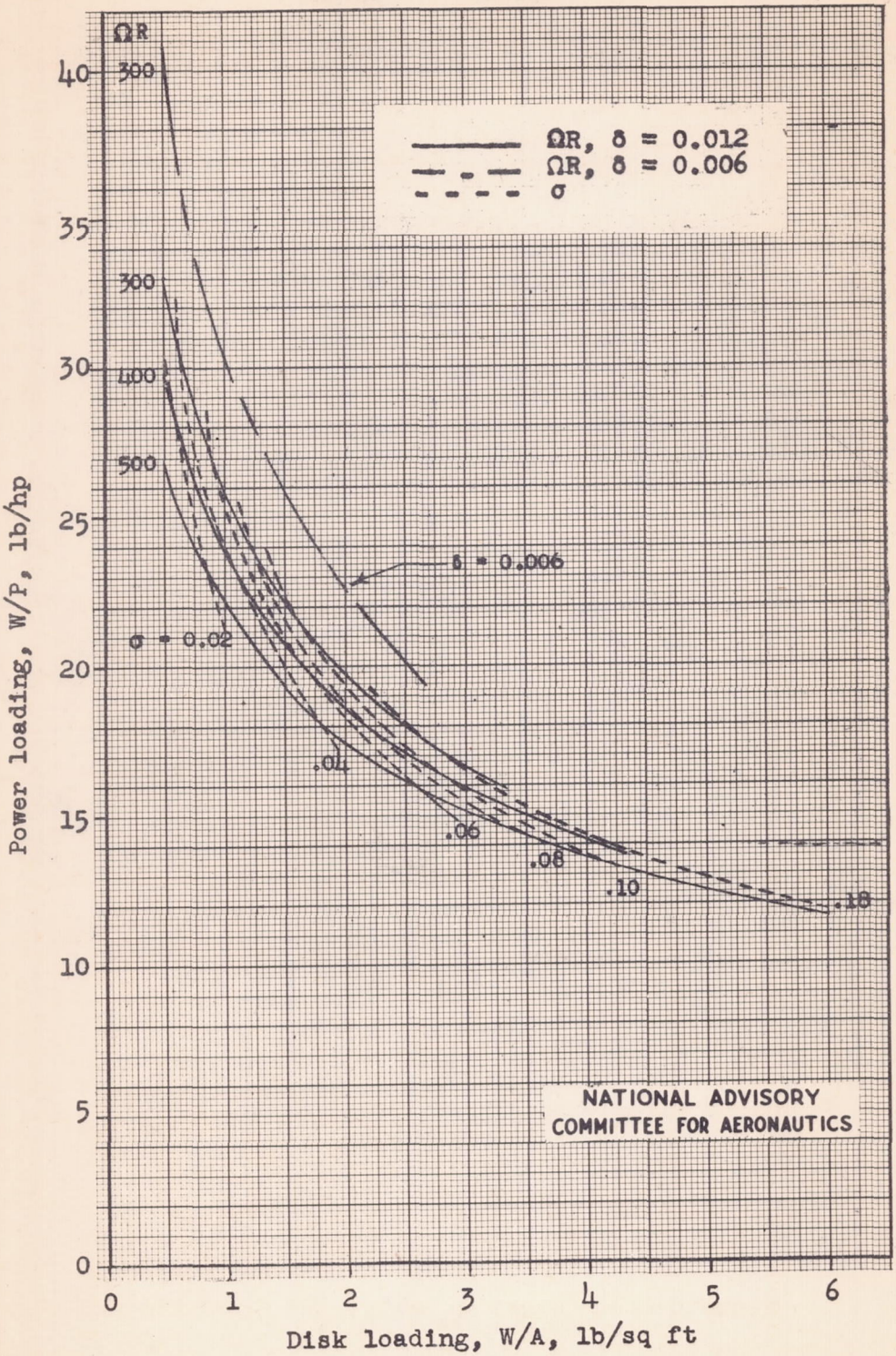

Figure 21.- Power-loading disk-loading performance chart for hovering helicopters at sea level with $\sigma Y_t^2 = 5740$.

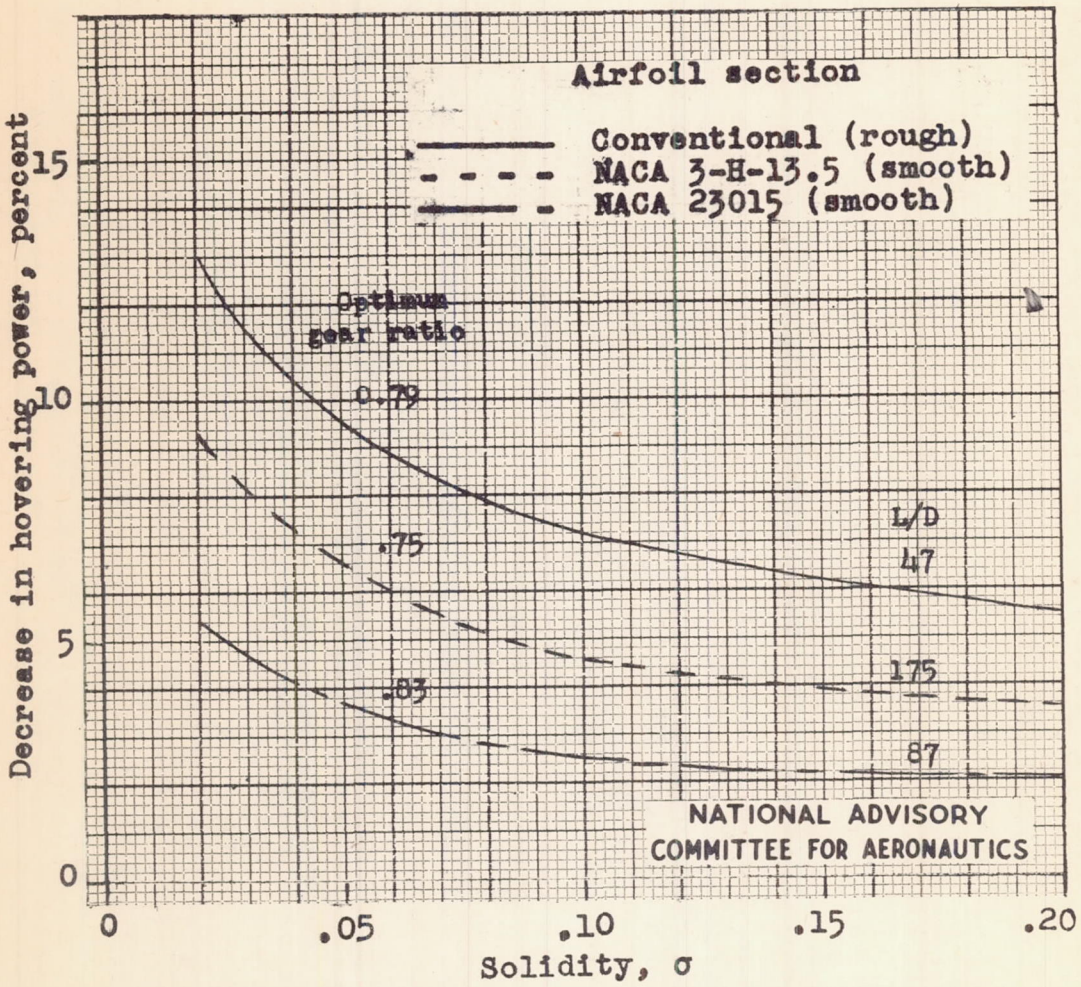

Figure 22.- Decrease in the power required for hovering by use of a rotor-speed-reduction gear.